AD-A116 588 NAVAL CIVIL ENGINEERING LAB PORT HUENEME CA F/G 8/10
AN ENERGETICS TOTAL LOAD SEDIMENT TRANSPORT MODEL FOR A PLANE S--ETC(U)
APR 82 J A BAILARD
UNCLASSIFIED NCEL-TN-1626 NL

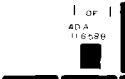

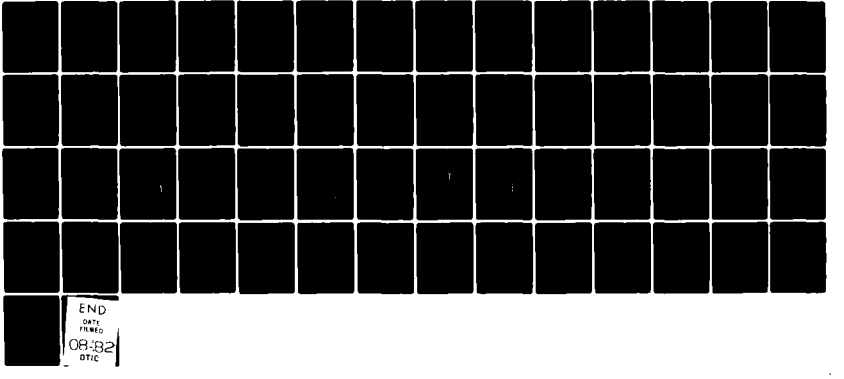

TECHNICAL NOTE

TN NO: N-1626

TITLE: AN ENERGETICS TOTAL LOAD SEDIMENT TRANSPORT MODEL FOR A PLANE SLOPING BEACH

AUTHOR: J. A. Bailard

DATE: April 1982

SPONSOR: Naval Civil Engineering Laboratory

PROGRAM NO: ZR000-01-183

NAVAL CIVIL ENGINEERING LABORATORY
PORT HUENEME, CALIFORNIA 93043

Unclassified

SECURITY CLASSIFICATION OF THIS PAGE (When Data Entered)

REPORT DOCUMENTATION PAGE		READ INSTRUCTIONS BEFORE COMPLETING FORM
1 REPORT NUMBER TN-1626	2 GOVT ACCESSION NO AD-A116588 DN187254	3 RECIPIENT'S CATALOG NUMBER
4 TITLE (and Subtitle) AN ENERGETICS TOTAL LOAD SEDIMENT TRANSPORT MODEL FOR A PLANE SLOPING BEACH		5 TYPE OF REPORT & PERIOD COVERED Final; Oct 1980 – Sep 1981 6 PERFORMING ORG REPORT NUMBER
7 AUTHOR(s) J. A. Bailard		8 CONTRACT OR GRANT NUMBER(s)
9 PERFORMING ORGANIZATION NAME AND ADDRESS NAVAL CIVIL ENGINEERING LABORATORY Port Hueneme, California 93043		10 PROGRAM ELEMENT PROJECT TASK AREA & WORK UNIT NUMBERS 61152N; ZR000-01-183
11 CONTROLLING OFFICE NAME AND ADDRESS NAVAL CIVIL ENGINEERING LABORATORY Port Hueneme, California 93043		12 REPORT DATE April 1982 13 NUMBER OF PAGES 65
14 MONITORING AGENCY NAME & ADDRESS(if different from Controlling Office)		15 SECURITY CLASS (of this report) Unclassified 15a DECLASSIFICATION DOWNGRADING SCHEDULE

16 DISTRIBUTION STATEMENT (of this Report)

Approved for public release; distribution unlimited.

17 DISTRIBUTION STATEMENT (of the abstract entered in Block 20, if different from Report)

18 SUPPLEMENTARY NOTES

19 KEY WORDS (Continue on reverse side if necessary and identify by block number)

Sediment transport, surfzone, model, longshore transport rate, equilibrium beach profile.

20 ABSTRACT (Continue on reverse side if necessary and identify by block number)

Bagnold's energetics-based total load sediment transport model for streams is used as a basis for the development of a total load model of time-varying sediment transport over a plane sloping bed. In both the bedload and suspended load, the transport rate vectors are found to be composed of a velocity-induced component directed parallel to the instantaneous velocity vector and a gravity-induced component directed downslope. The model is applied to idealized surfzone conditions, leading to estimates of the local longshore and on-offshore

(continued)

DD FORM 1 JAN 73 1473 EDITION OF 1 NOV 65 IS OBSOLETE

Unclassified

SECURITY CLASSIFICATION OF THIS PAGE (When Data Entered)

20. Continued

sediment transport rates as well as the equilibrium beach slope, as a function of the local wave and current conditions. The model is combined with a nonlinear longshore current model and is spatially integrated to obtain predictions of the total longshore transport rate as a function of the incident wave conditions. The results support the general form of the wave power equation except that the wave power coefficient is no longer constant but is instead a complex function of the incident wave and beach characteristics.

Library Card

Naval Civil Engineering Laboratory
AN ENERGETICS TOTAL LOAD SEDIMENT TRANSPORT MODEL FOR A PLANE SLOPING BEACH (Final), by
J. A. Bailard
TN-1626 65 pp illus April 1982 Unclassified

1. Sediment transport 2. Beach profile I. ZR000-01-183

Bagnold's energetics-based total load sediment transport model for streams is used as a basis for the development of a total load model of time-varying sediment transport over a plane sloping bed. In both the bedload and suspended load, the transport rate vectors are found to be composed of a velocity-induced component directed parallel to the instantaneous velocity vector and a gravity-induced component directed downslope. The model is applied to idealized surfzone conditions, leading to estimates of the local longshore and on-offshore sediment transport rates as well as the equilibrium beach slope, as a function of the local wave and current conditions. The model is combined with a nonlinear longshore current model and is spatially integrated to obtain predictions of the total longshore transport rate as a function of the incident wave conditions. The results support the general form of the wave power equation except that the wave power coefficient is no longer constant but is instead a complex function of the incident wave and beach characteristics.

CONTENTS

INTRODUCTION

Waves reaching a coastline are observed to break, releasing their energy and momentum within the narrow confines of the surfzone. This waveborne momentum flux gives rise to a longshore current, which contributes to the longshore sediment transport along the beach. Under equilibrium conditions, the longshore sediment transport takes place with no effect on the existing beach bathymetry. If interrupted, however, rapid alteration of the shoreline can occur, which may jeopardize nearshore structures. Recognizing the importance of these processes to Navy operations, the Independent Research program of the Naval Civil Engineering Laboratory sponsored a study to develop improved models to predict the magnitude and distribution of the longshore sediment transport rate as a function of incident wave and beach characteristics.

Present longshore current models are relatively well-developed, being based on a momentum balance between the longshore component of waveborne momentum flux and the bottom and lateral shear stresses associated with the longshore current. Early longshore current models (Bowen, 1969; Longuet-Higgins, 1970) assumed near normal wave angle incidence and weak longshore current strength in order to simplify their mathematical solution. Later models, such as those by Thornton (1970), James (1974), Liu and Dalrymple (1978), and Ostendorf and Madsen (1979), assumed arbitrary sized incident wave angles and longshore current strengths.

Present longshore sediment transport models are less well-developed. In general, these models reflect two distinct approaches: an energetics approach and a traction approach. The former includes models by Inman and Bagnold (1963), Komar (1971, 1977), Thornton (1973), Bowen (1981), and Bailard and Inman (1981), while the latter includes models by Bijker (1971), Swart (1976), and Madsen and Grant (1976). In both cases, these

approaches are based on adaptations of stream flow sediment transport models. The energetics approach, which is used in this report, is based on the stream transport model developed by Bagnold (1963, 1966).

Bagnold's energetics-based sediment transport model assumes that the sediment is transported in two distinct modes, differing by the way the sediment grains are supported. Sediment transported as bedload is supported by the bed via grain-to-grain interactions, while sediment transported as suspended load is supported by the stream fluid via turbulent diffusion. In both modes, energy is expended by the stream in transporting the sediment load. Bagnold, comparing the stream to a machine, defined the sediment transport efficiency as the ratio of the rate of energy expended in transporting either the bedload or the suspended load divided by the total rate of energy production of the stream.

For steady, two-dimensional stream flow, Bagnold (1963) developed the following total load sediment transport equation

$$i = i_B + i_S = \left(\frac{\varepsilon_B}{\tan\phi - \tan\beta} + \frac{\varepsilon_S}{\frac{W}{\bar{u}} - \tan\beta} \right) \omega \qquad (1)$$

where i = total immersed weight sediment transport rate (composed of the sum of the bedload transport rate, i_B, and the suspended load transport rate, i_S)

ω = rate of energy production of the stream

$\bar{u}$ = mean velocity of the stream

$\tan\beta$ = slope of the stream bed

ϕ = internal angle of friction of the sediment

W = fall velocity of the sediment

ε_B = bedload load efficiency

ε_S = suspended load efficiency

For stream flow conditions, Bagnold (1966) found that $\varepsilon_B \cong 0.13$ and $\varepsilon_S \cong 0.01$.

For oscillatory flows, such as those found in the surfzone, Bagnold (1963) developed an alternative but related sediment transport equation. Bagnold reasoned that the oscillatory wave motion acts to move the sediment back and forth in an amount proportional to the local rate of energy dissipation. Although no net transport results from this motion, a steady current of arbitrary strength, when superimposed on the wave-induced oscillatory motion, is free to transport the sediment in the steady current's direction. This conceptual model resulted in the following sediment transport equation

$$i_\theta = K' \omega \frac{u_\theta}{u_m} \tag{2}$$

where ω = local rate of energy dissipation

u_m = magnitude of the oscillatory water velocity

u_θ = steady current in the θ direction

i_θ = time-averaged, immersed weight, sediment transport rate in the θ direction

K' = Bagnold's oscillatory transport rate coefficient

Equation 2 has been used in the development of a number of longshore transport models, including those by Inman and Bagnold (1963), Komar (1971, 1977), and Thornton (1973). Inman and Bagnold's model is currently the most widely accepted and is equivalent in form to the equation recommended by the U.S. Army Corps of Engineers (Anonymous, 1973). Inman and Bagnold's model linearly relates the total spatially integrated, immersed weight, longshore transport rate, I_ℓ, to what has been erroneously (Longuet-Higgins, 1972) termed the longshore component of wave energy flux per unit length of beach, P_ℓ. The latter is defined as

$$P_\ell = (E\ C\ n)_b \sin\alpha_b \cos\alpha_b \tag{3}$$

where E = wave energy per unit length of crest

C = wave phase velocity

n = wave energy transport function

α_b = incident breaker angle

b = subscript that denotes the value at the breakpoint

The resulting longshore transport equation, termed the wave power equation, is expressed as

$$I_\ell = K P_\ell \tag{4}$$

where K is a dimensionless constant. Komar and Inman (1970) found that when K = 0.77, Equation 4 best fits the field data from 13 sand tracer experiments performed at El Moreno Beach, Mexico, and Silver Strand Beach, California.

Despite the general acceptance of Equations 2 and 4, their development is only loosely based on Bagnold's stream transport model (Equation 1). The latter suggests that an attempt should be made to differentiate between the bedload and suspended load transports within the surfzone and, in addition, the local bedslope should have some influence on the sediment transport rate. Physical reasoning also suggests that the time-averaging procedure implied by Equation 2 should be considered more carefully. Bailard and Inman (1981) and Bowen (1981) have attempted to correct some of these difficulties. Bailard and Inman used Bagnold's stream-based bedload model to derive a general form bedload equation that is valid for time-varying flow over an arbitrarily oriented sloping bottom. Their equation reduces to Bagnold's bedload equation for steady, two-dimensional stream flow. When applied to the surfzone, Bailard and Inman's results suggest that Equation 2 is only valid for weak longshore currents and near normal wave incidence (when suspended sediment transport is neglected).

Bowen (1981) applied Bagnold's total load sediment transport equation to the problem of on-offshore sediment transport on beaches. After generalizing Bagnold's total load Equation 1 for the special case of normally incident waves and steady on-offshore currents (no longshore currents), Bowen used Stokes second order wave theory and Longuet-Higgins' (1953) bottom streaming solutions to predict the equilibrium beach profile as a function of the incident wave characteristics. His results support observations that steep beaches are coarse-grained and flat beaches are fine-grained. Moreover, small, long-period waves cause a beach to accrete and large, short-period waves cause a beach to erode. Finally, a null-point hypothesis is supported.

At the present time, there is considerable uncertainty concerning the relative importance of bedload versus suspended load sediment transport within the surfzone. While in natural streams the suspended sediment transport rate generally dominates the bedload transport rate, field measurements suggest that in the surfzone, the suspended sediment transport rate accounts for less than 20% of the total (Komar, 1978). These measurements, however, implicitly assume that all sediment transported within approximately 10 cm of the bottom is bedload. In stream flow, however, the bedload transport is generally believed to take place within a few millimeters of the stationary bed. As a consequence, it would seem that much of the surfzone sediment transport presently considered to be bedload may, in fact, be suspended load. This hypothesis is supported by Bowen's (in press) on-offshore transport model, which suggests that the relative importance of the two sediment transport rates is a function of the orbital velocity magnitude divided by the sediment fall velocity, u_m/W.

The purpose of this report is to present a total load (bedload and suspended load) sediment transport model, developed for time-varying flow over an arbitrarily sloping planar bed. The model is similar to Bailard and Inman's (1981) bedload transport model in that it predicts the local, nearbottom sediment transport rate as a function of the nearbottom water velocity vector. For present purposes, nearbottom is

considered to be that region near the bottom where the velocity distribution is nearly logarithmic (see the Appendix). The model is similar to Bowen's (1981) model in that Bagnold's total load stream transport model (Equation 1) is used as a working hypothesis. The model is specialized for idealized surfzone conditions consisting of steady longshore and on-offshore currents in addition to an oscillatory wave-induced current having a local wave angle. The model is found to predict the local equilibrium beach slope as well as the local longshore sediment transport rate. In addition, the model is combined with Ostendorf and Madsen's (1979) longshore current model to predict the magnitude and distribution of the longshore sediment transport rate. A discussion of the model's limitations can be found in the concluding remarks.

DEVELOPMENT OF A TIME-VARYING TOTAL LOAD SEDIMENT TRANSPORT EQUATION

Consider the time-varying flow of water with vector velocity $\vec{u}_t$ moving over a plane sloping bed of cohesionless sediment. Figure 1 shows the x-axis is directed upslope and the y-axis is directed cross-slope. The magnitude of the slope is $\tan\beta$, and the velocity $\vec{u}_t$ has an arbitrary orientation relative to the x-axis but is coplanar with the x-y plane. The shear stress on the bed, $\vec{\tau}_t$, is assumed to be described by

$$\vec{\tau}_t = \rho\, c_f \left|\vec{u}_t\right| \vec{u}_t \tag{5}$$

where ρ = water density

c_f = drag coefficient for the bed

t = subscript that denotes a time-varying quantity

Similarly, the local rate of energy dissipation, ω_t, is assumed to be equal to

$$\omega_t = \rho c_f \left|\vec{u}_t\right|^3 \tag{6}$$

Note that for simplicity, any phase difference between the bed stress and the nearbottom fluid velocity is neglected.

Following Bailard and Inman (1981), the local immersed weight sediment transport rate, $\vec{i}_t$, is assumed to be a time-varying vector quantity with the following form

$$\vec{i}_t = \left(\vec{K}_{Bt} + \vec{K}_{St}\right)\omega_t \tag{7}$$

where $\vec{K}_{Bt}$ and $\vec{K}_{St}$ are the dimensionless time-varying vectors associated with the bedload and suspended load transport rates, respectively. Assuming the bedload transport to behave as a granular-fluid shear layer, Bailard and Inman (1981) found that

$$\vec{K}_{Bt} = \frac{\varepsilon_B}{\tan\phi}\left(\frac{\vec{u}_t}{\left|\vec{u}_t\right|} - \frac{\tan\beta}{\tan\phi}\hat{i}\right) \tag{8}$$

where ε_B = bedload efficiency

$\tan\phi$ = internal coefficient of friction of the sand

Equation 8 suggests that the bedload transport rate vector is composed of two components, one directed parallel to the instantaneous velocity vector and the other directed downslope.

Bagnold's (1963, 1966) conceptual model of suspended sediment transport in streams is relatively simple. He reasoned that the stream supports the suspended sediment via turbulent diffusion. While suspended, the sediment grains move downstream with nearly the local fluid velocity. At the same time, however, they are also falling vertically relative to the local supporting fluid with a fall velocity, W. In equilibrium, the center of mass of the suspended load must remain at a constant height above the stream bed; thus, the transport process extracts energy from the stream in an amount equal to the product of the immersed weight of

the suspended sediment and the sediment fall velocity. Using his analogy of the stream as a sediment transporting machine, Bagnold assumed that the power expended in transporting the suspended sediment is a constant fraction, ε_S, of the total power produced by the stream, ω. Extending this conceptual model to time-varying flow over an arbitrarily sloping planar bed, it can be shown (see the Appendix) that

$$\vec{K}_{S_t} = \varepsilon_S \frac{|\vec{u}_t|}{w} \left(\frac{\vec{u}_t}{|\vec{u}_t|} - \varepsilon_S \tan\beta \frac{|\vec{u}_t|}{w} \hat{i} \right) \tag{9}$$

Similar to the bedload transport rate, the suspended sediment transport rate vector is seen to consist of two components, one directed parallel to the instantaneous velocity vector and the other directed downslope. The latter is associated with the downslope component of the immersed weight of the suspended sediment.

Combining Equations 6, 7, 8, and 9, and time-averaging over a wave period T, where

$$\langle \quad \rangle = \frac{1}{T} \int_0^T \left(\quad \right) dt \tag{10}$$

then the following total load sediment transport equation is obtained

$$\langle \vec{i}_t \rangle = \rho c_f \frac{\varepsilon_B}{\tan\phi} \left(\langle |\vec{u}_t|^2 \vec{u}_t \rangle - \frac{\tan\beta}{\tan\phi} \langle |\vec{u}_t|^3 \rangle \hat{i} \right) + \rho c_f \frac{\varepsilon_S}{w} \left(\langle |\vec{u}_t|^3 \vec{u}_t \rangle - \frac{\varepsilon_S}{w} \tan\beta \langle |\vec{u}_t|^5 \rangle \hat{i} \right) \tag{11}$$

Bagnold's stream-based total load sediment transport equation is seen to be a special case of Equation 11, since both equations are equal when $\tan\beta << 1$ and $\vec{u}_t = -\bar{u}\,\hat{i}$. Equation 11 is also equivalent to Bowen's (1981) initial equation for on-offshore sediment transport conditions

($\vec{u}_t = |\vec{u}_t| \hat{i}$), except for the extra factor ε_s in the final term. This difference is of particular importance in relation to the equilibrium beach slope, which will be discussed more fully.

LITTORAL SEDIMENT TRANSPORT

Due to its general form, Equation 11 is not particularly useful unless nearbottom water velocity measurements are available. These measurements have recently become possible with the development of robust electromagnetic current meters (Cunningham et al., 1979). For modeling purposes, however, it is desirable to be able to express Equation 11 in terms of a steady current, $\bar{u}$, oriented at an angle θ to the beach normal and an oscillatory wave-induced velocity, $\tilde{u}$, oriented at an angle α to the beach normal. Figure 1 shows the instantaneous velocity vector, $\vec{u}_t$, may be expressed in terms of its x and y components

$$\vec{u}_t = (\tilde{u}\cos\alpha + \bar{u}\cos\theta)\,\hat{i} + (\tilde{u}\sin\alpha + \bar{u}\sin\theta)\,\hat{j} \qquad (12)$$

Observation (Huntley, 1976) has shown that while the wave-induced velocity is by definition oscillatory ($\langle\tilde{u}\rangle = 0$), it is not symmetrically distributed in time. Instead, there is a brief high-velocity onshore flow followed by a longer but less intense offshore flow. As a consequence, the third and fifth oscillatory velocity moments, $\langle\tilde{u}^3\rangle$ and $\langle\tilde{u}^5\rangle$, are nonzero. Following Bailard and Inman (1981) or Bowen (1981), this asymmetry may be expressed by assuming the following approximate form for $\tilde{u}$

$$\tilde{u} \cong u_m \cos\sigma t + u_{m2} \cos 2\sigma t + \ldots. \qquad (13)$$

where $u_m > u_{m2}$, etc., and $\sigma = 2\pi/T$.

Equations 12 and 13 may be used to evaluate the time-averaged scalar and vector quantities in Equation 11. After considerable manipulation, the following expressions are obtained for the on-offshore, $\langle i_x \rangle$, and the longshore, $\langle i_y \rangle$, sediment transport rates

$$\langle i_x \rangle = \rho\, c_f\, u_m^3 \left\{ \frac{\varepsilon_B}{\tan\phi} \left[\psi_1 \cos\alpha + \delta_u^3 + \delta_u \left(\frac{1}{2} + \cos^2\alpha + \delta_v^2 \right) + \delta_v \sin\alpha \cos\alpha - \frac{\tan\beta}{\tan\phi} (u3)^* \right] + \frac{u_m}{w} \varepsilon_S \left[\psi_2 \cos\alpha + \delta_u (u3)^* \right] - \frac{u_m^2}{w^2} \varepsilon_S^2 \tan\beta\, (u5)^* \right\} \tag{14}$$

$$\langle i_y \rangle = \rho\, c_f\, u_m^3 \left\{ \frac{\varepsilon_B}{\tan\phi} \left[\psi_1 \sin\alpha + \delta_v^3 + \delta_v \left(\frac{1}{2} + \sin^2\alpha + \delta_u^2 \right) + \delta_u \sin\alpha \cos\alpha \right] + \frac{u_m}{w} \varepsilon_S \left[\psi_2 \sin\alpha + \delta_v (u3)^* \right] \right\} \tag{15}$$

where the relative steady current strengths δ, δ_u, and δ_v are defined as

$$\delta = \frac{\bar{u}}{u_m} \tag{16a}$$

$$\delta_u = \frac{\bar{u}}{u_m} \cos\theta \tag{16b}$$

$$\delta_v = \frac{\bar{u}}{u_m} \sin\theta \tag{16c}$$

The velocity moments ψ_1 and ψ_2 are defined as

$$\psi_1 = \langle \tilde{u}^3 \rangle / u_m^3 \tag{17}$$

$$\psi_2 = \langle \left|\vec{u}\right|^3 \tilde{u} \rangle / u_m^4 \qquad (18)$$

and the integrals (u3)* and (u5)* are defined as

$$(u3)^* = \frac{1}{T} \int_0^T (\delta^2 + 2\,\delta \cos(\theta-\alpha) \cos\sigma t + \cos^2\sigma t)^{3/2}\, dt \qquad (19)$$

$$(u5)^* = \frac{1}{T} \int (\delta^2 + 2\,\delta \cos(\theta-\alpha) \cos\sigma t + \cos^2\sigma t)^{5/2}\, dt \qquad (20)$$

Bailard and Inman (1981) obtained approximate analytic expressions for the integral (u3)* for the special cases of weak and strong steady currents. In the present development, however, both (u3)* and (u5)* are left unevaluated. Later, when the model is combined with Ostendorf and Madsen's (1979) longshore current model in order to predict the distribution of the longshore sediment transport rate as a function of the incident wave conditions, these integrals are evaluated using a five-point Gaussian quadrature equation, as used by Ostendorf and Madsen, i.e.,

$$\begin{aligned}(u3)^* = {} & 0.118\,[(u3)^*(\sigma t=2.99) + (u3)^*(\sigma t=0.147)] \\ & + 0.239\,[(u3)^*(\sigma t=2.42) + (u3)^*(\sigma t=0.725)] \\ & + 0.284(u3)^*(\sigma t=1.57)\end{aligned} \qquad (21)$$

Equation 21 can be shown to be accurate to within ±2% for $\delta \leq 2$ and $(\theta-\alpha) \leq 90$ degrees. Alternatively, (u3)* and (u5)* may be interpolated from Figures 2 and 3.

Equations 14 and 15 are still unsuitable for modeling purposes because of the presence of the two skewness terms ψ_1 and ψ_2. Following Bailard and Inman (1981), however, ψ_1 and ψ_2 may be eliminated from Equation 15 by assuming that the beach is in local on-offshore equilibrium ($\langle i_x \rangle = 0$). Under this condition, Equation 14 becomes

$$\frac{\varepsilon_B}{\tan\phi}\,\psi_1\,\cos\alpha + \frac{u_m}{W}\,\varepsilon_S\,\psi_2\,\cos\alpha = \frac{\varepsilon_B}{\tan\phi}\left[\frac{\tan\beta}{\tan\phi}\,(u3)^* - \delta_u^3 - \delta_u\left(\frac{1}{2} + \cos^2\alpha + \delta_v^2\right) - \delta_v \sin\alpha\,\cos\alpha\right] - \frac{u_m}{W}\,\varepsilon_S\,\delta_u\,(u3)^* + \frac{u_m^2}{W^2}\,\varepsilon_S^2\,\tan\beta\,(u5)^* \qquad (22)$$

Combining Equations 22 and 15, one obtains

$$\langle i_y\rangle = \rho\,c_f\,u_m^3\left\{\frac{\varepsilon_B}{\tan\phi}\left[\delta_v^3 + \delta_u^2\,\delta_v + \frac{\delta_v}{2} + \left(\frac{\tan\beta}{\tan\phi}\,(u3)^* - \delta_v^2\,\delta_u - \frac{\delta_u}{2} - \delta_u^3\right)\tan\alpha\right] + \frac{u_m}{W}\,\varepsilon_S\left[\delta_v\,(u3)^* - \delta_u(u3)^*\,\tan\alpha\right] + \frac{u_m^2}{W^2}\,\varepsilon_S^2\,\tan\beta\,(u5)^*\,\tan\alpha\right\} \qquad (23)$$

Finally, when it is assumed that $\delta_u << \delta_v$, then Equation 23 reduces to the desired longshore transport equation

$$\langle i_y\rangle = \rho\,c_f\,u_m^3\left\{\frac{\varepsilon_B}{\tan\phi}\left[\delta_v^3 + \frac{\delta_v}{2} + \frac{\tan\beta}{\tan\phi}\,(u3)^*\,\tan\alpha\right] + \frac{u_m}{W}\,\varepsilon_S\,\delta_v\,(u3)^* + \frac{u_m^2}{W^2}\,\varepsilon_S^2\,\tan\beta\,(u5)^*\,\tan\alpha\right\} \qquad (24)$$

Equation 24 can be compared with Bagnold's oscillatory transport Equation 2, which is rewritten for longshore transport conditions as

$$\langle i_y \rangle = \frac{4}{3\pi} \rho \, c_f \, K' \, u_m^3 \, \delta_v \tag{25}$$

Comparing Equations 24 and 25, both equations are equal if

$$K' = \frac{3\pi}{4} \frac{\varepsilon_B}{\tan\phi} \left[\frac{1}{2} + \delta_v^2 + \frac{\tan\beta}{\tan\phi} \frac{(u3)^*}{\delta_v} \tan\alpha \right]$$

$$+ \frac{3\pi}{4} \frac{u_m}{W} \varepsilon_S \left[(u3)^* + \frac{u_m}{W} \varepsilon_S \tan\beta \frac{(u5)^*}{\delta_v} \tan\alpha \right] \tag{26}$$

The above equation suggests that instead of K' being constant, it is a function of δ_v, α, $\tan\beta$, and u_m/W. This is in accordance with our earlier hypothesis based on Bagnold's stream transport (Equation 1). Note that for the special case when δ_v, α, $\tan\beta$, and u_m/W are very small, then Bailard and Inman's (1981) result is recovered

$$K' = \frac{3\pi}{8} \frac{\varepsilon_B}{\tan\phi} \tag{27}$$

With typical surfzone conditions ($\tan\beta = 0.10$, $\alpha = 10$ degrees, $\varepsilon_B = 0.21$, and $\varepsilon_S = 0.025$) assumed, Figure 4 shows Bagnold's transport coefficient K' as a function of the dimensionless longshore current strength, δ_v, and the ratio, u_m/W. The coefficient K' is seen to be a strong function of both δ_v and u_m/W. Only for weak longshore currents and small values of u_m/W does K' approach the constant value expressed by Equation 27.

EQUILIBRIUM BEACH SLOPES

In addition to predicting the longshore sediment transport rate, the present model can be used to predict the equilibrium beach slope as well. By definition, a beach slope is in local equilibrium when the divergence of the time-averaged sediment transport rate vector is zero, i.e.,

$$\frac{\partial \langle i_x \rangle}{\partial x} + \frac{\partial \langle i_y \rangle}{\partial y} = 0 \tag{28}$$

When a two-dimensional, steady-state beach is assumed, then $\langle i_y \rangle$ = constant and $\langle i_x \rangle = 0$. If the beach slope tanβ is small, then the latter condition applied to Equation 14 yields

$$\tan\beta = \left\{ \frac{\varepsilon_B}{\tan\phi} \left[\psi_1 \cos\alpha + \delta_u^3 + \delta_u \delta_v^2 + \delta_u \left(\frac{1}{2} + \cos^2\alpha \right) + \delta_v \sin\alpha \cos\alpha \right] + \frac{u_m}{W} \varepsilon_S \left[\psi_2 \cos\alpha + \delta_u (u3)^* \right] \right\} \cdot \left\{ \frac{\varepsilon_B}{\tan^2\phi} (u3)^* + \frac{u_m^2}{W^2} \varepsilon_S^2 (u5)^* \right\}^{-1} \tag{29}$$

For normal wave incidence, negligible longshore currents, and weak on-offshore currents, Equation 29 becomes

$$\tan\beta = \frac{\frac{\varepsilon_B}{\tan\phi} \left(\psi_1 + \frac{3}{2} \delta_u \right) + \frac{u_m}{W} \varepsilon_S \left(\psi_2 + \frac{4}{3\pi} \delta_u \right)}{\frac{4}{3\pi} \frac{\varepsilon_B}{\tan^2\phi} + \frac{16}{15\pi} \frac{u_m^2}{W^2} \varepsilon_S^2} \tag{30}$$

Equation 30 is closely related to the equilibrium beach slope equation developed by Bowen (1981). The two equations are most easily compared if the skewness factors, ψ_1 and ψ_2, and the relative on-offshore current strength, δ_u, are estimated from Stoke's second-order wave theory and Longuet-Higgins' (1953) bottom drift model, respectively. Following Bowen (1981), we assume that

$$\tilde{u} = u_m \cos\sigma t + \frac{3}{4} \frac{u_m^2}{C} \sinh^{-2} kh \cos 2\sigma t \tag{31}$$

and

$$\bar{u}\cos\theta = \frac{u_m^2}{C} \tag{32}$$

where C = wave phase velocity

k = wave number

h = local water depth

Combining Equations 12, 17, 18, 31, and 32, the skewnesses, ψ_1 and ψ_2, are found to be equal to

$$\psi_1 = \frac{9}{16}\frac{u_m}{C}\sinh^{-2}kh \tag{33}$$

and

$$\psi_2 = \frac{12}{5\pi}\frac{u_m}{C}\sinh^{-2}kh + \frac{4}{\pi}\frac{u_m}{C} \tag{34}$$

and the dimensionless on-offshore current strength, δ_u, is equal to

$$\delta_u = \frac{u_m}{C} \tag{35}$$

Combining Equations 30, 33, 34, and 35, the equilibrium beach slope equation then becomes

$$\tan\beta = \frac{\frac{\varepsilon_B}{\tan\phi}\left(\frac{27\pi}{64}\frac{u_m}{C}\sinh^{-2}kh + \frac{9\pi}{8}\frac{u_m}{C}\right) + \frac{u_m}{W}\varepsilon_S\left(\frac{9}{5}\frac{u_m}{C}\sinh^{-2}kh + 4\frac{u_m}{C}\right)}{\frac{\varepsilon_B}{\tan^2\phi} + \frac{4}{5}\frac{u_m^2}{W^2}\varepsilon_S^2} \tag{36}$$

The principal difference between Bowen's equilibrium beach slope equation and Equation 36 is that the latter has an ε_S^2 in the denominator instead of an ε_S. As a result, the slope effect in the suspended sediment

transport rate in Equation 36 is $1/\varepsilon_s$ or approximately 40 times less than in Bowen's equation. Predicted equilibrium beach slopes for strong suspension conditions are thus significantly greater in the present model.

Following Bowen (1981) and noting that

$$\frac{u_m}{C} = \frac{ak}{\sin kh} \tag{37a}$$

$$\frac{u_m}{W} = \frac{a\sigma}{W \sinh kh} \tag{37b}$$

$$k \cong \frac{k_o}{\tanh^{1/2} k_o h} \tag{37c}$$

where k_o is the deepwater wave number, then the modified beach slope, $\tan\beta/ak_o$, may be plotted as a function of the parameters $k_o h$ and $a\sigma/W$ (Figure 5). The resulting figure is qualitatively very similar to the figure obtained by Bowen. Both figures show that the beach slope increases with decreasing depth, increasing fall velocity, and increasing wave period. All three features are generally observed in nature. A null point hypothesis is also supported in that sediment coarser than the equilibrium grain size moves onshore, while sediment finer than the equilibrium moves offshore. The biggest discrepancy between the present model and that which is observed in nature is in the magnitude of the predicted equilibrium beach slope in shallow water. The present model significantly overpredicts slopes that are actually observed or that are predicted by Bowen's model. The evidence, however, is inconclusive in evaluating either model because Stoke's second-order wave theory is not valid in shallow water. As a result, it is best to consider Equation 34 or Figure 5 as indicative only of trends and not of actual magnitudes of the equilibrium beach slope.

In principle, simultaneous measurements of nearbottom surfzone water velocities and surfzone beach profiles taken over a considerable length of time should be able to resolve this uncertainty. A preliminary analysis of field data from the Nearshore Sediment Transport Study at

Torrey Pines Beach suggests that autosuspension conditions can occur relatively frequently when using a model such as Bowen's, which is compatible with Bagnold's equations. This, of course, leads to momentary infinite offshore suspended sediment transport rates, which seems untenable. The present model avoids this problem for reasons discussed in the Appendix. A more comprehensive study of this question is needed, however, before any conclusions can be made.

The above discussion pertained only to normally incident waves with negligible longshore currents. Equation 29, however, permits an evaluation of the relative effects of wave angle incidence and longshore current strength on the local equilibrium beach slope. Due to the complexity of Equation 29, it is necessary to consider nominal surfzone conditions where $\varepsilon_B = 0.21$, $\varepsilon_S = 0.025$, $\psi_1 = 0.10$, $\psi_2 = 0.10$, and $\tan\phi = 0.63$. Figure 6 shows $\tan\beta$ plotted as a function of the relative longshore current strength, δ_v, and the local wave angle, α. It is evident that for these conditions, $\tan\beta$ is a strong function of the longshore current strength, decreasing with increasing δ_v for $\delta_v > 0.2$. The equilibrium beach slope is a somewhat weaker function of the local wave angle, α increasing slightly with increasing α for $\delta_v > 0.04$.

The sensitivity of the equilibrium beach slope to the longshore current strength suggests a mechanism for the formation of a breakpoint bar and trough. Field and laboratory observations of longshore currents suggest that the longshore current strength increases with distance from the shoreline until reaching a maximum near the breakpoint. It subsequently decreases with additional distance offshore. Figure 6 suggests that the effect of the longshore current on the equilibrium beach profile would be to flatten the profile in the area of the maximum longshore current (i.e., just inside the breakpoint). This flattening would, in effect, create a bar and trough type of feature, with the bar located seaward of the current maximum and the trough located shoreward of the maximum.

SURFZONE SEDIMENT TRANSPORT DISTRIBUTION AND INTEGRATED TOTAL

Equation 15 predicts the local total longshore transport rate as a function of the local wave-induced velocity magnitude, u_m, the local wave angle, α, and the local longshore current, δ_v. In order to predict the distribution of the longshore sediment transport rate across the surfzone as a function of the incident wave conditions, it is necessary to incorporate a longshore current model. A review of existing longshore current models suggests that Ostendorf and Madsen's (1979) model is most suitable for the present study. The important features of their model are that finite wave height, longshore current strength, and incident wave angle effects are incorporated, as are the effects of lateral momentum exchange.

Ostendorf and Madsen's (1979) longshore current model uses a similarity form of solution, where the fundamental solution is approximately equal to Longuet-Higgins' (1970) linear solution, and correction factors are included to account for the effects of finite longshore current strength, incident wave angle, and breaker height. The model has the following form

$$v = \lambda\, n_b \cos\alpha_b\, v_c v^* \tag{38}$$

where $v_c v^*$ = linear longshore current distribution

λ = finite current strength factor

n_b = factor equivalent to the wave energy transport function at the breakpoint

$\cos\alpha_b$ = finite incident wave angle factor

The dimensionless longshore current distribution, v^*, has the following form

$$v^* = C_1 \left(\frac{1 - C_2}{C_2 - C_3}\right) x^{*\,C_3} + C_1\, x^* \qquad (P \neq 0.4,\ x^* \leq 1) \tag{39}$$

$$v^* = C_1 \left(\frac{1 - C_3}{C_2 - C_3} \right) x^{*C_2} \qquad (P \neq 0.4,\ x^* > 1)$$

$$v^* = 0.26\, x^* - 0.71\, x^* \ln x^* \qquad (P = 0.4,\ x^* \leqq 1)$$

$$v^* = 0.26\, x^{*-1.71} \qquad (P = 0.4,\ x^* > 1)$$

where

$$C_1 = (1 - 2.5\, P)^{-1}$$

$$C_2 = -\frac{1}{8} - \left(\frac{1}{64} + \frac{1}{P} \right)^{1/2} \qquad (40)$$

$$C_3 = -\frac{3}{4} + \left(\frac{9}{16} + \frac{1}{P} \right)^{1/2}$$

The dimensionless distance from the shoreline, x^* (see Figure 1), is defined as

$$x^* = \frac{x - x_S}{x_B - x_S} \qquad (41)$$

where x_S and x_B are the positions of the shoreline and breakpoint, respectively. The lateral mixing parameter, P, is defined as

$$P = \frac{\pi\, \Gamma\, \tan\Delta}{2\, c_f} \qquad (42)$$

where Γ is a lateral mixing coefficient and $\tan\Delta$ is equal to the average beach slope, $\tan\beta$, modified to account for the wave setup, i.e.,

$$\tan\Delta = \tan\beta \left(1 + \frac{3}{8} \gamma_b^2 \right)^{-1} \qquad (43)$$

Based on laboratory velocity profiles, Ostendorf and Madsen found that $\Gamma \cong 0.13$.

In deriving Equation 38, it is assumed that the local wave-height-to-water-depth ratio, $\gamma = H/h$, has the following distribution

$$\gamma = \gamma_b \qquad (x^* \leq 1)$$
$$\gamma = \gamma_b \left(\frac{h_b}{h}\right)^{5/4} \qquad (x^* > 1) \tag{44}$$

In addition, the characteristic longshore current magnitude, v_c, is defined as

$$v_c = \delta_c \, u_{mb} \tag{45}$$

where the magnitude of the oscillatory wave velocity at the breakpoint, u_{mb}, is obtained from shallow water wave theory, i.e.,

$$u_{mb} \approx \frac{\gamma}{2}\sqrt{g \, h_b} \tag{46}$$

and the relative longshore current strength, δ_c, is defined as

$$\delta_c = \frac{5\pi \tan\Delta \sin\alpha_b}{8 \, c_f} \tag{47}$$

Ostendorf and Madsen present an iterative procedure for estimating the breakpoint values of H, h, and n as a function of the incident wave conditions. In addition, the finite current parameter, λ, is obtained iteratively from the parameters n_b, α_b, δ_c, and P.

Combining the longshore current Equation 38 and the longshore transport Equation 24, and noting that

$$u_m = u_{mb} \frac{\gamma}{\gamma_b} \sqrt{x^*} \tag{48}$$

and

$$\delta_v = \delta_c \lambda n_b \cos\alpha_b \frac{\gamma_b}{\gamma} \frac{v^*}{\sqrt{x^*}} \tag{49}$$

then the longshore transport rate distribution becomes

$$\begin{aligned} \langle i_y \rangle = \rho c_f u_{mb}^3 \Bigg\{ & \frac{\varepsilon_B}{\tan\phi} \left[\frac{\delta_c}{2} \lambda n_b \cos\alpha_b \left(\frac{\gamma}{\gamma_b}\right)^2 v^* x^* \right. \\ & \left. + \delta_c^3 \lambda^3 n_b^3 \cos^3\alpha_b v^{*3} + \frac{\tan\beta}{\tan\phi} (u3)^* \left(\frac{\gamma}{\gamma_b}\right)^3 x^{*3/2} \tan\alpha \right] \\ & + \frac{u_{mb}}{W} \varepsilon_S \left[\delta_c \lambda n_b \cos\alpha_b (u3)^* \left(\frac{\gamma}{\gamma_b}\right)^3 v^* x^{*3/2} \right] \\ & + \frac{u_{mb}^2}{W^2} \varepsilon_S^2 \tan\beta \left[(u5)^* \left(\frac{\gamma}{\gamma_b}\right)^5 x^{*5/2} \tan\alpha \right] \Bigg\} \end{aligned} \tag{50}$$

Equation 50 can be normalized by dividing by the bedload transport rate at the breakpoint under weak current, near normal wave incidence conditions with no lateral mixing, i_c, where

$$i_c = \frac{1}{2} \rho c_f \frac{\varepsilon_B}{\tan\phi} n_b \delta_c u_{mb}^3 \cos\alpha_b \tag{51}$$

Following this procedure, Equation 50 becomes

$$<i_y^*> = \frac{<i_y>}{i_c} = \lambda \left(\frac{\gamma}{\gamma_b}\right)^2 v^* x^* + 2 \delta_c^2 \lambda^3 n_b^2 \cos^2\alpha_b \, v^{*3}$$

$$+ \frac{2}{\delta_c \, n_b \cos\alpha_b} \frac{\tan\beta}{\tan\phi} (u3)^* \left(\frac{\gamma}{\gamma_b}\right)^3 x^{*3/2} \tan\alpha$$

$$+ \frac{u_{mb}}{W} \frac{\varepsilon_S}{\varepsilon_B} \tan\phi \cdot \left[2 \lambda (u3)^* \left(\frac{\gamma}{\gamma_b}\right)^3 v^* x^{*3/2}\right]$$

$$+ \frac{u_{mb}^2}{W^2} \frac{\varepsilon_S^2}{\varepsilon_B} \tan\phi \tan\beta$$

$$\cdot \left[\frac{2}{\delta_c \, n_b \cos\alpha_b} \left(\frac{\gamma}{\gamma_b}\right)^5 (u5)^* x^{*5/2} \tan\alpha\right] \qquad (52)$$

Because of its complexity, Equation 52 is difficult to generalize in a simple manner. Nevertheless, assuming nominal surfzone conditions ($\tan\beta = 0.1$, $\lambda = 1.0$, $n_b = 1.0$, $\alpha_b = 10$ degrees, $\delta_c = 0.5$, $P = 0.2$, $\varepsilon_B = 0.21$, and $\varepsilon_S = 0.025$), the distribution of $<i_y^*>$ can be plotted as a function of the ratio u_{mb}/W (Figure 7). In Figure 7, several features can be seen. First, the profiles are a strong function of the parameter u_{mb}/W. Increasing values of u_{mb}/W strongly increases the total load sediment transport rate. Another feature of the profiles is the slope discontinuity at the breakpoint ($x^* = 1$). This feature is a curiosity associated with the slope discontinuity in the distribution of γ at this point. In reality, this discontinuity would not exist. A final feature of the profiles is that the relative location of the sediment transport rate maximum is seaward of the maximum longshore current.

The ratio of the normalized suspended sediment transport rate divided by the normalized bedload transport rate, i_S^*/i_B^*, is also a function of the distance from the beach. Figure 8 shows a plot of the distribution of the ratio i_S^*/i_B^* as a function of the ratio u_{mb}/W for the same surfzone conditions as those assumed for Figure 7. As might be expected, the ratio increases with distance offshore until the breakpoint, and then begins to decrease. Another anticipated result is that the ratio increases throughout the nearshore with increasing values of u_{mb}/W.

A more easily measured quantity than the longshore transport rate distribution is the spatially integrated total longshore transport rate, I_ℓ, defined as

$$I_\ell = \int_{-\infty}^{x_s} \langle i_y \rangle \, d_x = \frac{h_b \, i_c}{\tan\Delta} \int_0^\infty \langle i_y^* \rangle dx^* \tag{53}$$

Substituting Equations 50, 51, and 52 into Equation 53 and noting that

$$E_b = \frac{1}{8} \rho \, g \, H_b^2 \tag{54}$$

and

$$(C \, n)_b = \frac{2 \, n_b}{\gamma_b} u_{mb} \tag{55}$$

then Equation 53 becomes

$$I_\ell = \frac{5\pi}{16} \frac{\gamma_b \, \varepsilon_B}{\tan\phi} \int_0^\infty \langle i_y^* \rangle \, dx^* \, (E \, C \, n)_b \sin\alpha_b \cos\alpha_b \tag{56}$$

Comparing Equation 56 with the wave power Equation 4, the wave power coefficient K is seen to have the following form

$$K = \frac{5\pi}{16} \frac{\gamma_b \, \varepsilon_B}{\tan\phi} \int_0^\infty \langle i_y^* \rangle \, dx^* \tag{57}$$

Instead of being constant, Equation 57 suggests that K is a complex function of the incident wave conditions, the beach slope, and the sediment size. For the special case of negligible lateral mixing, weak longshore current strength, near normal breaker angle, small breaker height, and small water-velocity-to-fall-velocity ratio, K becomes a constant, K_o, where

$$K_o = \frac{5\pi}{48} \frac{\gamma_b \varepsilon_B}{\tan\phi} \tag{58}$$

Using K_o to normalize the wave power coefficient, we obtain

$$K^* = \frac{K}{K_o} = 3 \int_0^\infty \langle i_y^* \rangle \, dx^* \tag{59}$$

Again the normalized wave power coefficient, K^*, is a complex function of surfzone parameters. To illustrate its behavior, we assume nominal surfzone conditions where $\tan\Delta = 0.1$, $n_b = 1.0$, $\lambda = 1.0$, $\gamma_b = 1.0$, $P = 0.2$, $\varepsilon_B = 0.21$, and $\varepsilon_S = 0.025$. Figure 9 shows K^* plotted as a function of the relative longshore current strength, δ_c, the breaker angle, α_b, and the ratio u_{mb}/W. For small values of u_{mb}/W, K^* is seen to be nearly independent of δ_c or α_b. As the ratio u_{mb}/W increases, however, K^* also increases, becoming a function of δ_c and α_b. Finally, K^* decreases with increasing longshore current strength and increases with increasing breaker angle. These results will vary, however, for different input conditions.

The relative overall fraction of suspended sediment transport versus bedload transport, I_S/I_B, may also be plotted as a function of δ_c, α_b, and u_{mb}/W. Assuming the same surfzone conditions, Figure 10 shows that the relative transport ratio behaves exactly as the normalized wave power coefficient, a result to be expected because for large values of u_{mb}/W, most of the sediment transport is by suspension.

MODEL CALIBRATION

Laboratory and field data available for calibrating and evaluating the longshore transport model are relatively limited. Greer and Madsen (1978) reviewed existing field data and concluded that Komar and Inman's (1970) sand tracer studies at El Moreno and Silver Strand Beaches were

the most reliable. Very recently, a series of large-scale field experiments, termed the Nearshore Sediment Transport Study, have been conducted at two Southern California beaches. Details of the studies may be found in Gable (1979, 1981); however, the data from these studies are only now becoming available for analysis and thus will not be considered in the present study.

Laboratory data are also very limited. In the present case, measurements must include the incident wave conditions, the mean longshore current, the equilibrium beach slope, and the total longshore sediment transport rate. Following the study by Ostendorf and Madsen (1979), selected data from Saville (1950) and Shay and Johnson (1951) will be used in the present study. A summary of the field and laboratory data used in the present study may be found in Table 1.

The numerical calibration procedure is as follows. In reference to Equations 50, 52, and 56, the present longshore transport model has three unknown parameters: the drag coefficient, c_f; the bedload efficiency, ε_B; and the suspended load efficiency, ε_S. Using Ostendorf and Madsen's longshore current model, the drag coefficient is estimated from the measured mean longshore current. In the process, estimates for E_b, n_b, α_b, λ, γ_b, δ_c, P, and u_{mb} are also obtained. These parameters completely define the longshore current distribution. Next, the distribution of $\langle i_y^* \rangle$ is calculated as a function of ε_B and ε_S using Equation 52. Integrating this distribution via Equation 57, the estimated wave power coefficient, K_{est}, is calculated as a function of ε_B and ε_S yielding

$$K_{est} = \varepsilon_B K_1 + \varepsilon_S K_2 + \varepsilon_S^2 K_3 \tag{60}$$

where

$$K_1 = \frac{5\pi}{16} \frac{\gamma_b}{\tan\phi} \int_0^\infty \left[\lambda \left(\frac{\gamma}{\gamma_b} \right)^2 v^* x^* + 2 \delta_c^2 \lambda^3 n_b^2 \cos^2\alpha_b v^{*3} + \frac{2}{\delta_c n_b \cos\alpha_b} \frac{\tan\beta}{\tan\phi} (u3)^* \left(\frac{\gamma}{\gamma_b} \right)^3 x^{*3/2} \tan\alpha \right] dx^* \tag{61}$$

$$K_2 = \frac{5\pi}{16}\frac{u_{mb}}{w}\int_0^{\infty}\left[2\,\lambda\,(u3)^*\left(\frac{\gamma}{\gamma_b}\right)^3 v^*\,x^{*3/2}\right]dx^* \qquad (62)$$

$$K_3 = \frac{5\pi}{16}\frac{u_{mb}^2}{w^2}\tan\beta\int_0^{\infty}\left[\frac{2}{\delta_c\,n_b\,\cos\alpha_b}\,(u5)^*\,x^{*5/2}\,\tan\alpha\right]dx^* \qquad (63)$$

Estimates of K_1, K_2, and K_3 for all data sets are included in Table 1. With use of these estimates, a nonlinear least-square procedure (Draper and Smith, 1966) was used to estimate the values of the bedload efficiency, $\hat{\varepsilon}_B$, and the suspended load efficiency, $\hat{\varepsilon}_S$, from the measured values of the wave power coefficient, K_{obs}. This procedure requires constructing a two-dimensional contour plot of the mean square error, $S(\varepsilon_B, \varepsilon_S)$, defined as

$$S(\varepsilon_B,\varepsilon_S) = \frac{1}{n-2}\sum_{j=1}^{n}(K_{obs}-K_{est})^2 \qquad (64)$$

where n is the total number of data pairs.

While following the above procedures, it was found that the data from El Moreno Beach appeared to be anomolous. When compared with the other data, the measured values of K appeared to be roughly three times too large. As a consequence, it was decided to calibrate the model using only the field data from Silver Strand Beach and the laboratory data. The resulting least-square contour plot is shown in Figure 11. The least-square estimates, $\hat{\varepsilon}_B$ and $\hat{\varepsilon}_S$, were found to be equal to 0.2[illegible] and 0.025, respectively. Figure 11 also shows the 95% confidence contour, suggesting that the 95% bounds on $\hat{\varepsilon}_B$ and $\hat{\varepsilon}_S$ are $0 < \varepsilon_B < 0.44$ and $0.016 < \hat{\varepsilon}_S < 0.031$. Figure 12 shows a plot of the relative errors, K_{obs}/K_{est}, as a function of the estimated wave power coefficient. Clearly the relative error of the calibration data is approximately equally distributed about one, suggesting that $\hat{\varepsilon}_B$ and $\hat{\varepsilon}_S$ are unbiased.

Figure 12 also shows the relative errors of the El Moreno Beach data. These errors show that the measured wave power coefficients are seriously underestimated. One explanation for this behavior is that the transport processes at El Moreno Beach may have been significantly different than those at Silver Strand Beach and in the laboratory. In particular, the steep beach face and small wave heights produced waves which broke on the beach face itself. It would be expected that swash zone transport processes would predominate under these conditions. Observations have shown that the swash zone is a region of abnormally high suspended sediment concentrations and transport, and as a result, it appears plausible that the present model would tend to underestimate transport in this region.

The least square estimates, $\hat{\varepsilon}_B$ and $\hat{\varepsilon}_S$, are encouraging because they are similar in size to the values estimated by Bagnold for stream flow. Bagnold (1966) analyzed data from laboratory and field measurements of sediment transport rates in channel flow and estimated that $\varepsilon_B \cong 0.13$ and $\varepsilon_S \cong 0.01$. The fact that the present estimates are roughly twice these values is not improbable. In the case of the bedload efficiency, most of the transport in the surfzone is suspension, and the total transport rate is relatively insensitive to the estimated value of the bedload efficiency. This is reflected in the relatively large error bounds on $\hat{\varepsilon}_B$. Bagnold's stream-based estimate clearly falls within the allowable error. In the case of the suspended sediment efficiency, Bagnold's estimate does not fall within the bounds of the present estimate. This may reflect the different turbulence structure of the surfzone relative to the stream flow. In fact, the surfzone turbulence simulation model developed by Johns (1980) suggests that the turbulence energy density near the bed is dominated by the turbulence energy production at the face of the bore as opposed to that generated by the shear at the bed. The latter is clearly the dominant process in stream flow. As a result, it is not surprising that the suspended sediment efficiency is enhanced in the surfzone.

CONCLUDING REMARKS

The present sediment transport model incorporates a wide range of simplifying assumptions. While these assumptions are necessary due to the complexity of actual surfzone processes, it is believed that they have some physical basis.

A number of assumptions used in the present model share a common basis with many longshore current models. These assumptions include: the use of linear shallow water wave theory, linear breaker height variation across the surfzone, and a bed stress formulation which is quadratic in velocity and has a zero phase lag. Some of these assumptions are better justified than others. Guza and Thornton (1980) have shown that linear wave theory does a surprisingly good job of predicting oscillatory velocity magnitudes from local water depth measurements. Laboratory measurements (Bowen et al., 1968) have shown that for normal incident waves, a linear breaker height variation across the surfzone is reasonably accurate. The quadratic stress formulation, however, appears more open to question. Laboratory and theoretical studies of purely oscillatory turbulent boundary layers have shown that the nearbottom water velocity lags the bed shear stress in phase by approximately 30 degrees (Fisher et al., 1974; Jonsson and Carleson, 1976; Jonsson, 1980; Smith, 1977; Grant and Madsen, 1979). The applicability of these studies inside the surfzone is unknown. The bore propagation model developed by Johns (1980), however, appears to be more realistic of surfzone conditions. This model suggests that a quadratic shear stress model with a constant drag coefficient underestimates the magnitude of peak bed stresses which occur under the face of the bore. Despite these problems, the quadratic shear stress model is utilized in most longshore current models because it is well-suited to a vertically integrated formulation.

The present energetics-based sediment transport model also uses vertically integrated equations. As a consequence, no details of the vertical distribution of suspended sediment flux are resolved. A further consequence of using vertically integrated equations is that the sediment

transports are assumed to respond to the nearbottom water velocity in an instantaneous, quasi-steady manner. This assumption is probably valid for bedload transport (except for a phase lag) because the thickness of the bedload layer is small and can respond quickly to the instantaneous bed shear stress. The suspended sediment transport, however, is distributed over a greater layer thickness, typically on the order of several centimeters. Assuming a layer thickness, ℓ, and a sediment fall velocity, W, the characteristic time constant for the sediment transport layer is ℓ/W, which is typically on the order of 1 to 2 seconds. For most planar beaches with incident wave periods of roughly 8 seconds, it appears that the quasi-steady assumption is reasonable.

For rippled bottoms, the situation is more complicated. Inman and Bowen (1963) found that in the laboratory, simple phase-independent sediment transport models are inadequate for combined oscillatory and steady flow over a rippled bottom. They found such flows to exhibit a complex phase-dependent behavior associated with vortex-induced suspension occurring over the ripple crests. As a consequence, the present model is probably most useful in describing sediment transport inside the surfzone, where plane bed conditions usually prevail. Limiting the model to this region also minimizes the effects of neglecting the threshold stress condition for sediment transport due to the stronger steady currents found there.

Other uncertainties of the present model include the use of constant bedload and suspended load efficiency factors. Although constant values have been found to be adequate in steady stream flow (Bagnold, 1966), their adequacy in time-varying flow is unknown.

Despite the above limitations, the present model does exhibit certain behavior observed in nature. This is most evident in its predictions of the equilibrium beach slope. The present study substantiates Bowen's (1981) results; coarse-grained beaches are steeper than fine-grained beaches and short-period, large-amplitude waves are erosive. It is also encouraging that the present model produces results similar to the wave power equation. To a large degree, however, this is the result of both approaches being based on energy considerations. Finally, the

fact that the bedload and suspended load efficiency factors estimated from surfzone data are similar in size to the values estimated from stream flow lends further credence to the model.

In closing, several comments can be made concerning improvements to the model. It is clear from the above discussion that many of the details of the sediment transport processes are hidden by the use of vertically integrated equations. In part, this is justified by the resulting mathematical simplicity and by the lack of adequate data to validate more sophisticated boundary layer models. The latter, however, is changing due to the advent of more sophisticated sensors. Clearly, if significant progress is to be made, models which predict the details of the boundary layer flow field and sediment concentration distribution will have to be developed for the surfzone. If simple predictive equations are desired, it is always best to develop simplifying assumptions based on a knowledge of the complete solution.

REFERENCES

Anonymous (1973). Shore protection manual, U.S. Army Corps of Engineers, Coastal Engineering Research Center. 1973.

Bagnold, R. A. (1963). "Mechanics of marine sedimentation," in The Sea: Ideas and Observations, volume 3. New York, N.Y., Interscience Publishers, 1963, pp 507-528.

Bagnold, R. A. (1966). An approach to the sediment transport problem from general physics, U.S. Geological Survey, Professional Paper No. 422-I. Washington, D.C., 1966.

Bailard, J. A., and D. L. Inman (1981). "An energetics bedload transport model for a plane sloping beach; local transport," Journal of Geophysical Research, vol 86, no. 3, 1981, pp 2035-2043.

Bijker, E. W. (1971). "Longshore transport computations," Proc. ASCE Journal of Waterways, Harbors and Coastal Engineering, WW4, Nov 1971.

Bowen, A. J. (1969). "The generation of longshore currents on a plane beach," Journal of Marine Research, volume 27, no. 2, 1969, pp 206-215.

Bowen, A. J. (1981). "Simple models of nearshore sedimentation; beach profiles and longshore bais," in Proceedings of the Conference on Coastline of Canada, Halifax, 1978, Geological Survey of Canada.

Bowen, A. J., D. L. Inman, and V. P. Simmons (1968). "Wave set-down and set-up," Journal of Geophysical Research, vol 73, no. 8, 1968, pp 2569-2577.

Cunningham, P. M., R. T. Guza, and R. L. Lowe (1979). "Dynamics calibration of electromagnetic flow meters," I.E.E.E. Oceans, vol 79, 1979, pp 298-301.

Draper, N. R., and H. Smith (1966). Applied regression analysis. New York, N.Y., John Wiley, 1966.

Fisher, J., B. Johnson, and M. E. McCormick (1974). "Time dependent shear stress beneath a shoaling wave," in Proceedings of the International Symposium on Ocean Wave Measurements and Analysis, New Orleans, 1974, vol 1. New York, American Society of Civil Engineers, 1974, pp 799-816.

Gable, C. G. (1979). Report on data from the Nearshore Sediment Transport Study experiment at Torrey Pines Beach, California, November - December 1978, Institute of Marine Research, IMR Ref. No. 79-8. La Jolla, Calif., 1979.

Gable, C. G. (1981). Report on data from the Nearshore Sediment Transport Study experiment at Ledbetter Beach, Santa Barbara, CA, January - February 1980, Institute of Marine Research, IMR Ref. No. 80-5. La Jolla, Calif., 1981.

Grant, W. D., and O. S. Madsen (1979). "Combined wave and current interaction with a rough bottom," Journal of Geophysical Research, vol 84, no. C4, 1979, pp 1797-1808.

Greer, M. N., and O. S. Madsen (1978). "Longshore sediment transport data: A review," in Proceedings of the 16th Conference on Coastal Engineering. American Society of Civil Engineers, 1978.

Guza, R. T., and E. B. Thornton (1980). "Local and shoaled comparisons of sea surface elevations, pressures and velocities," Journal of Geophysical Research, vol 85, no. C3, 1980, pp 1524-1530.

Huntley, D. A. (1976). "Lateral and bottom forces on longshore currents," in Proceedings of the 15th Conference on Coastal Engineering, Honolulu, Hawaii, 1976. American Society of Civil Engineers, pp 645-659.

Inman, D. L., and R. A. Bagnold (1963). "Littoral processes," in The Sea: Ideas and Observations, volume 3. New York, N.Y., Interscience Publishers, 1963, pp 529-533.

Inman, D. L., and A. J. Bowen (1963). "Flume experiments on sand transport by waves and currents," in Proceedings of the Eighth Conference on Coastal Engineering. American Society of Civil Engineers, 1963, pp 137-150.

James, I. D. (1974). "A nonlinear theory of longshore currents," Estuarine and Coastal Marine Science, vol 2, 1974, pp 235-299.

Johns, B. (1980). "The modeling of the approach of bores to a shoreline," Coastal Engineering, vol 3, no. 3, 1980, pp 207-220.

Jonsson, I. G. (1980). "A new approach to oscillatory rough turbulent boundary layers," Ocean Engineering, vol 7, no. 1, 1980, pp 109-152.

Jonsson, I. G., and N. A. Carleson (1976). "Experimental and theoretical investigations in an oscillatory rough turbulent boundary layer," Journal of Hydraulic Research, vol 14, 1976, pp 45-60.

Komar, P. D. (1971). "The mechanics of sand transport on beaches," Journal of Geophysical Research, vol 76, no. 3, 1971, pp 713-721.

Komar, P. D. (1977). "Beach sand transport: Distribution and total drift," Proceedings of ASCE Journal of Waterways, Harbors and Coastal Engineering, WW4, May 1977, pp 225-239.

Komar, P. D. (1978). "Relative quantities of suspension versus bedload transport on beaches," Journal of Sedimentary Petroleum, vol 48, no. 3, 1978, pp 921-932.

Komar, P. D., and D. L. Inman (1970). "Longshore sand transport on beaches," Journal of Geophysical Research, vol 75, no. 30, 1970, pp 5914-5927.

Lui, P. L-F., and R. Dalrymple (1978). "Bottom frictional stresses and longshore currents due to waves with large angles of incidence," Journal of Marine Research, vol 37, no. 2, 1978, pp 357-375.

Longuet-Higgins, M. S. (1953). "Mass transport in water waves," Philosophical Transactions of the Royal Society, London, Series A, vol 245, 1953, pp 535-581.

Longuet-Higgins, M. S. (1970). "Longshore currents generated by obliquely incident sea waves, 2," Journal of Geophysical Research, vol 75, no. 33, 1970, pp 6790-6801.

Longuet-Higgins, M. S. (1972). "Recent progress in the study of longshore currents," in Waves on Beaches and Resulting Sediment Transport, R. E. Meyer, Editor. New York, N.Y., Academic Press, 1972, p. 462.

Madsen, O. S., and W. D. Grant (1976). Sediment transport in the coastal environment, Massachusetts Institute of Technology, Department of Civil Engineering, Ralph M. Parsons Laboratory, Report No. 241. 1976, p. 105.

Ostendorf, D. W., and O. S. Madsen (1979). An analysis of longshore currents and associated sediment transport in the surfzone, Massachusetts Institute of Technology, Department of Civil Engineering, Ralph M. Parsons Laboratory. Cambridge, Mass., 1979, p. 169.

Saville, T. (1950). "Model study of sand transport along an infinitely long, straight beach," Transactions, American Geophysical Union, vol 31, no. 4, 1950, pp 555-565.

Shay, E. A., and J. W. Johnson (1951). Model studies on the movement of sand transported by wave action along a straight beach, University of California, Department of Engineering, Institute of Engineering Research, Series 14, Issue 7. 1951, p. 58.

Smith, J. D. (1977). "Modeling of sediment transport on continental shelves," in The Sea: Ideas and Observations, volume 6. New York, N.Y., Interscience Publishers, 1977, pp 539-577.

Smith, J. D., and S. R. McLean (1977). "Spatially averaged flow over a wavy bottom," Journal of Geophysical Research, vol 82, no. 12, pp 1735-1746.

Swart, D. H. (1976). "Predictive equations regarding coastal transports," in Proceedings of the 15th Conference on Coastal Engineering. American Society of Civil Engineers, 1976.

Thornton, E. B. (1970). "Variation of longshore current across the surfzone," in Proceedings of the 12th Conference on Coastal Engineering. American Society of Civil Engineers, 1970, pp 291-308.

Thornton, E. B. (1973). "Distribution of sediment transport across the surfzone," in Proceedings of the 13th Conference on Coastal Engineering. American Society of Civil Engineers, 1973, pp 1049-1068.

Table 1. Data Relating Longshore Sediment Transport to Wave and Beach Characteristics

Run	T (sec)	H_b (cm)	α_b (deg)	n_b	γ_b	tanβ	u_{mb}/W	$\bar{v}$ (cm/sec)	I_ℓ (dynes/sec)	c_f	λ	P	K_1	K_2	K_3	K_{obs}
Saville Laboratory (grain diameter = 0.30 mm; w = 4.0 cm/sec)																
1	0.74	4.61	7.0	0.68	1.01	0.132	8.0	9.8	1,793	0.016	0.81	0.18	0.543	1.82	15.6	0.0085
2	0.85	4.61	6.4	0.59	1.05	0.133	8.1	8.2	3,094	0.015	0.84	0.17	0.551	1.81	18.6	0.165
3	0.94	4.73	6.0	0.54	1.07	0.133	8.3	7.6	4,803	0.014	0.85	0.18	0.554	1.85	20.9	0.255
4	1.00	4.71	5.8	0.51	1.08	0.133	8.3	6.4	4,372	0.016	0.88	0.16	0.565	1.87	24.9	0.247
5	0.74	5.06	7.3	0.71	1.00	0.133	8.3	12.2	2,302	0.013	0.78	0.22	0.539	1.94	13.5	0.0082
6	0.85	5.12	6.6	0.62	1.04	0.133	8.5	9.8	3,749	0.014	0.82	0.19	0.547	1.94	18.2	0.146
7	0.99	5.00	5.9	0.52	1.08	0.133	8.5	7.3	6,789	0.015	0.87	0.17	0.567	1.92	23.8	0.320
Shay and Johnson Laboratory (grain diameter = 0.30 mm; w = 4.0 cm/sec)																
1	1.08	5.06	5.7	0.48	1.09	0.116	8.7	7[a]	5,034	0.012	0.87	0.14	0.567	1.99	22.7	0.242
2	1.00	4.71	5.8	0.51	1.08	0.112	8.3	7[a]	5,665	0.012	0.86	0.14	0.555	1.90	19.2	0.320
3	0.86	5.18	6.6	0.63	1.03	0.096	8.5	7[a]	2,933	0.017	0.87	0.07	0.556	1.97	21.1	0.111
Komar El Moreno Beach (grain diameter = 0.60 mm; w = 9.5 cm/sec)																
1	2.75	39.3	9.8	0.53	1.07	0.138	10.7	50.0	45.1×10^5	0.0076	0.70	0.36	0.606	3.02	22.1	0.70
2	4.0	45.3	15.9	0.39	1.11	0.138	11.7	51.6	84.4×10^5	0.0091	0.68	0.28	0.631	3.26	48.7	0.80
3	3.4	31.7	18.9	0.38	1.11	0.138	9.8	43.0	25.7×10^5	0.0106	0.67	0.24	0.663	2.84	43.2	0.99
4	3.1	29.9	12.5	0.41	1.10	0.138	9.5	14.1	9.9×10^5	0.0358	0.88	0.074	0.710	2.27	99.0	1.00
5	4.5	40.5	7.9	0.32	1.12	0.138	11.0	22.4	14.6×10^5	0.0104	0.81	0.24	0.550	2.33	49.4	0.65
6	3.75	45.8	13.4	0.42	1.10	0.138	11.7	48.8	42.8×10^5	0.0092	0.70	0.29	0.607	3.12	42.4	0.63
7	4.9	47.7	2.2	0.32	1.12	0.138	12.0	16.9	6.1×10^5	0.0038	0.88	0.67	0.434	2.11	20.9	0.93
8	4.8	39.9	6.4	0.30	1.12	0.138	11.0	10.3	8.9×10^5	0.0214	0.94	0.12	0.660	2.54	10.5	0.68
9	2.9	31.4	3.4	0.45	1.10	0.138	9.7	7.2	2.9×10^5	0.0065	0.95	0.12	0.616	2.24	54.7	0.59
10	3.6	40.4	2.8	0.41	1.10	0.138	10.9	16.4	20.8×10^5	0.0014	0.90	0.41	0.485	2.13	22.3	1.20
Komar Silver Strand Beach (grain diameter = 0.175 mm; w = 2.0 cm/sec)																
1	11.0	144	5.0	0.35	0.844	0.34	86.5	55.9	30.2×10^5	0.014	0.74	0.11	0.423	17.0	238	0.40
2	10.6	82.7	6.1	0.27	0.848	0.034	65.5	14.6	47.1×10^5	0.0053	0.90	0.03	0.441	12.4	670	0.88
3	8.9	81.4	2.2	0.32	0.846	0.034	65.0	12.6	37.9×10^5	0.0026	0.93	0.06	0.422	12.1	265	0.70

[a]Assumed.

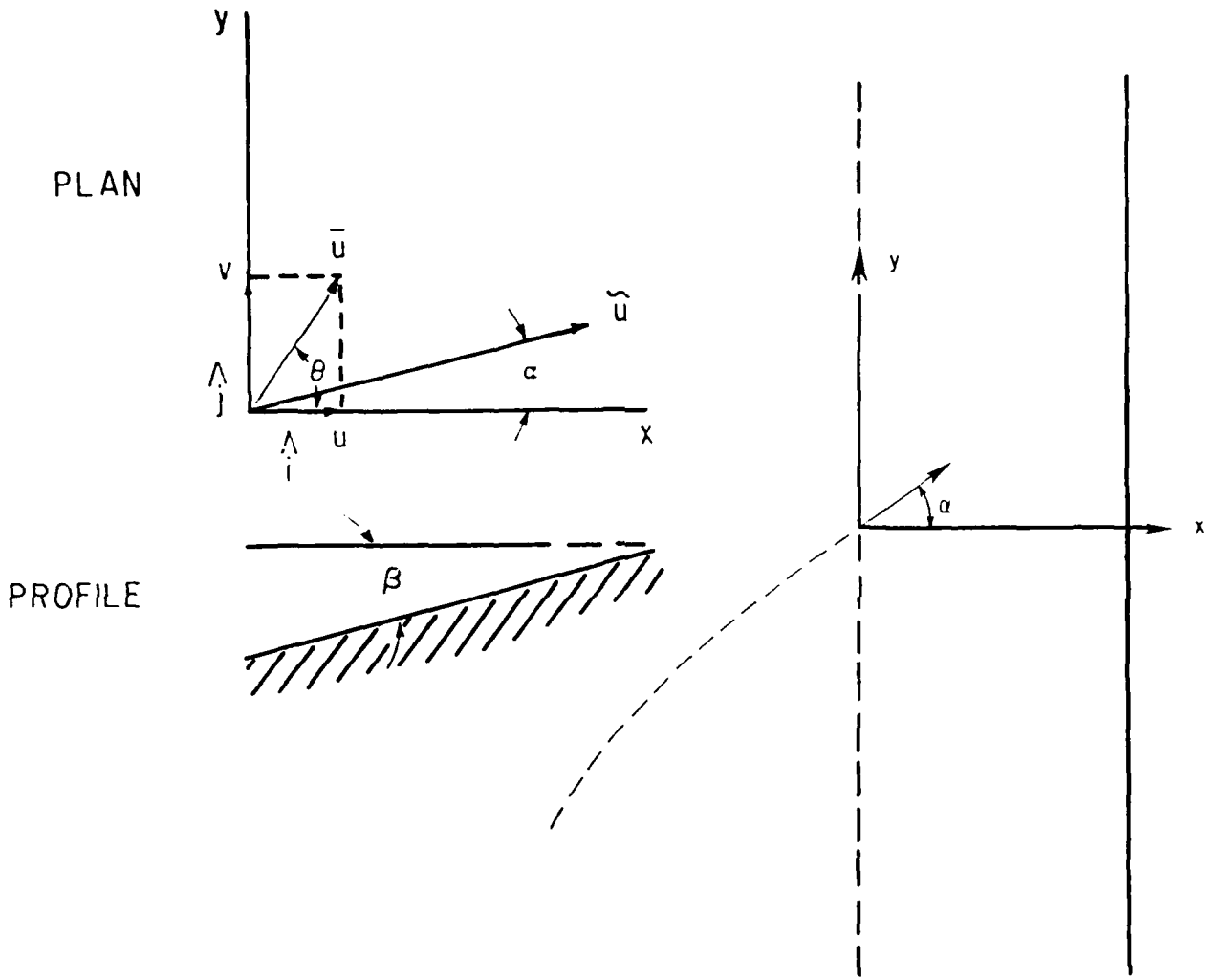

Figure 1. Schematic diagram showing the position of the beach, the breakpoint, and the steady and oscillatory water velocities, $\bar{u}$ and $\tilde{u}$, within the surfzone.

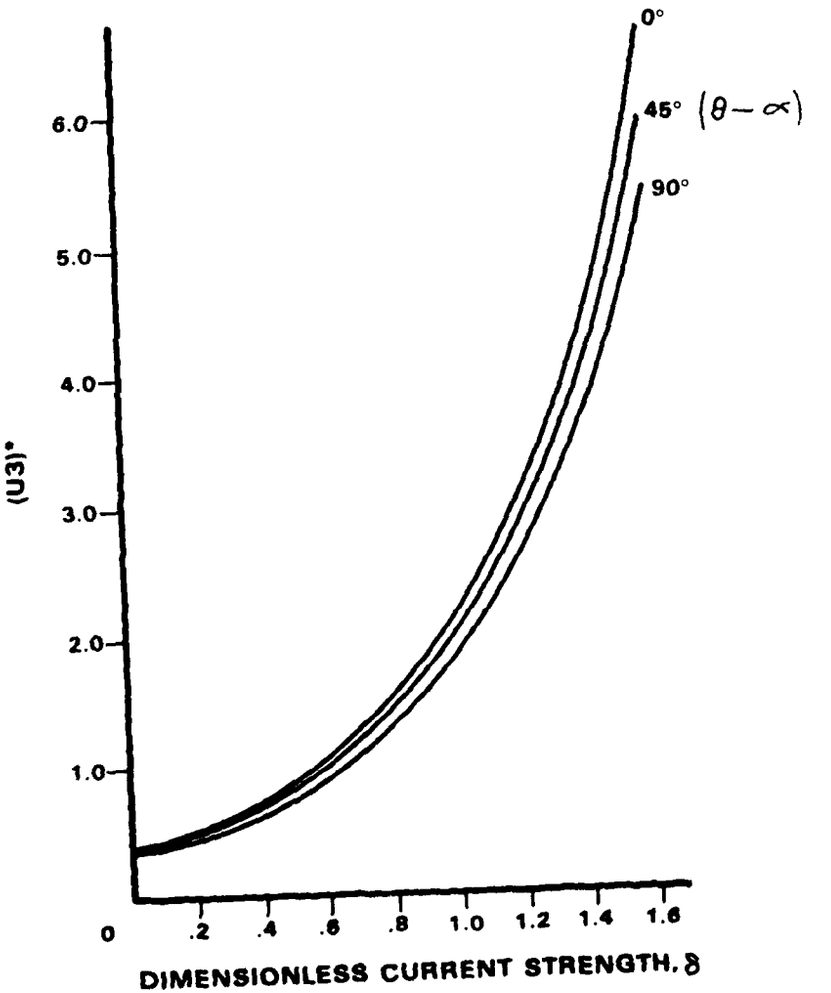

Figure 2. Relationship between the integral $(u3)^*$ and the dimensionless steady current strength, δ, for different angles between the steady and oscillatory water velocities, θ-α.

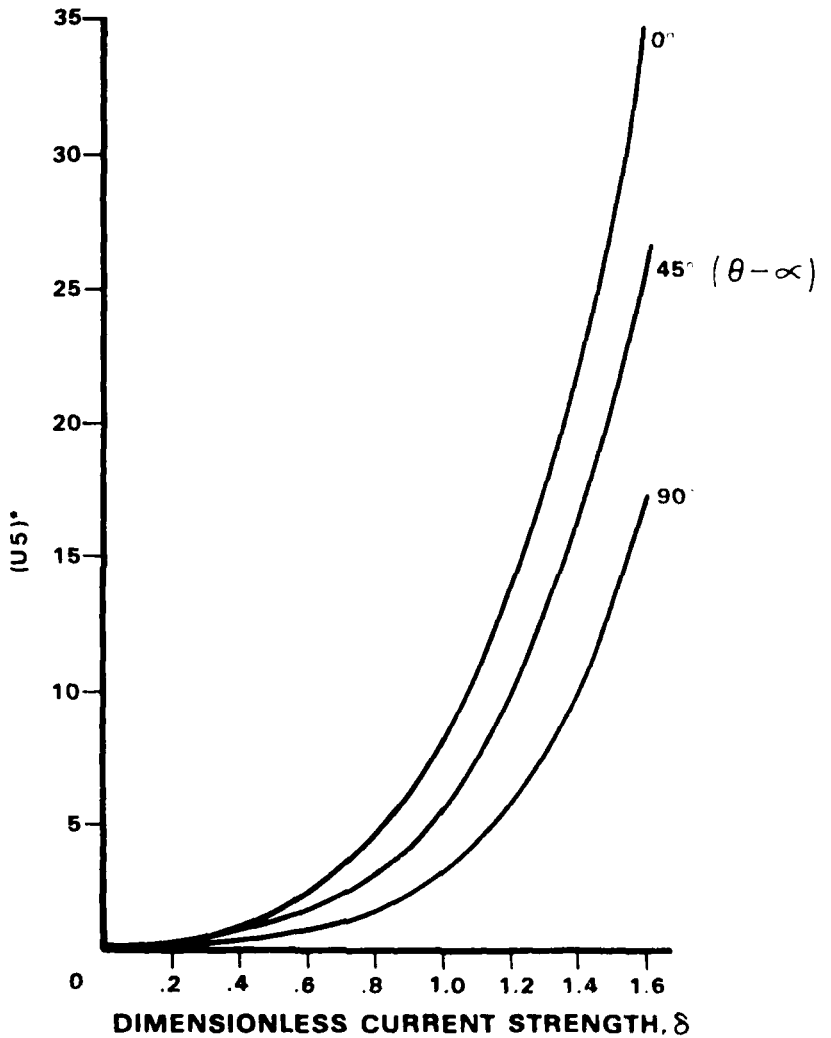

Figure 3. Relationship between the integral $(u5)^*$ and the dimensionless steady current strength, δ, for different angles between the steady and oscillatory water velocities, θ-α.

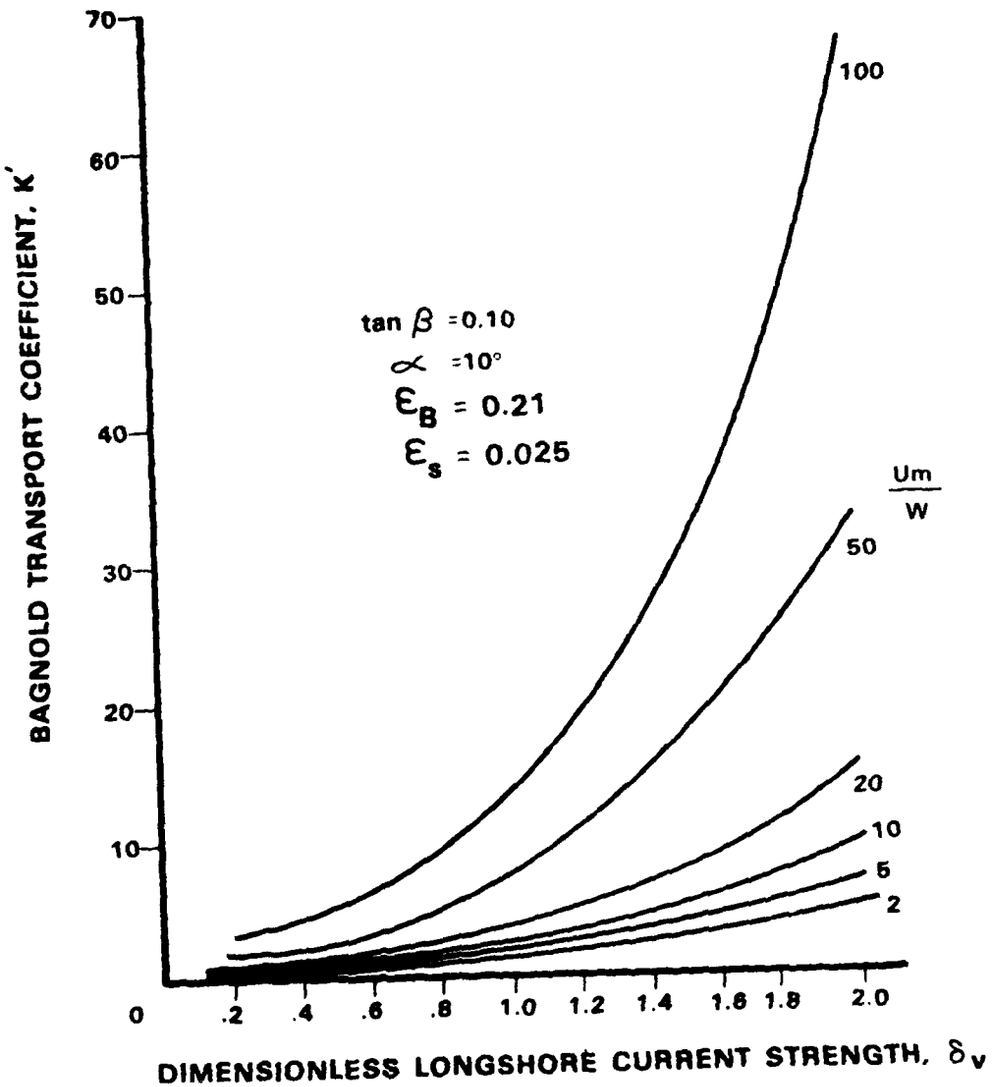

Figure 4. Relationship between Bagnold's oscillatory transport coefficient, K', and the dimensionless longshore current strength, δ_v, for different values of the velocity ratio u_m/W.

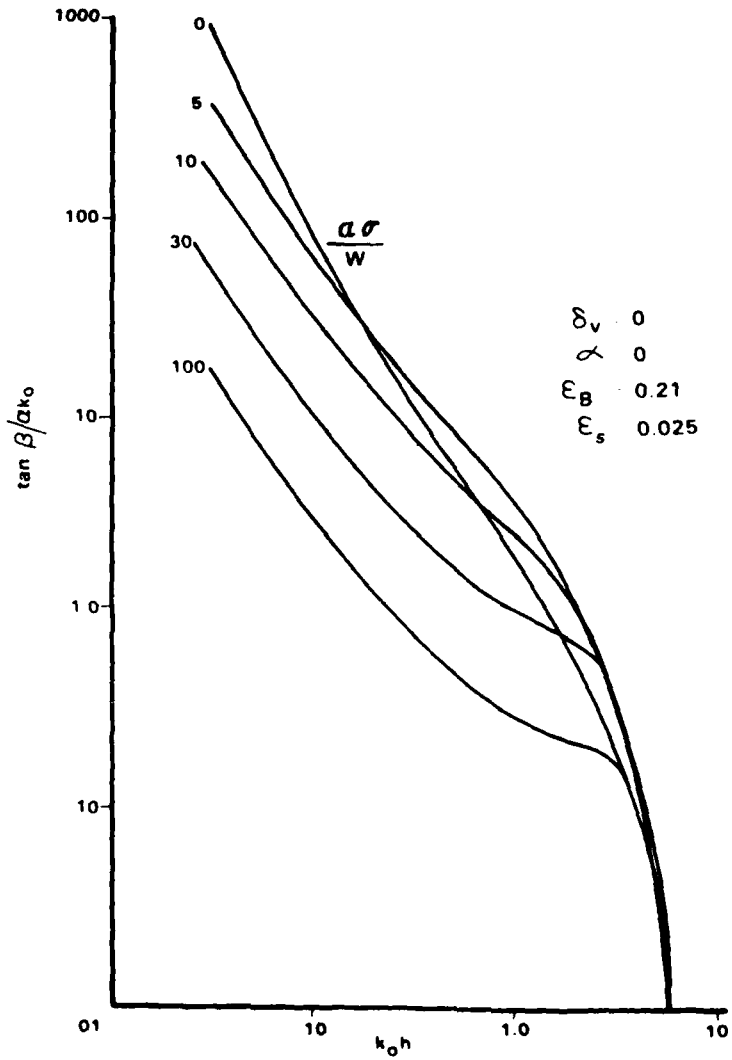

Figure 5. Relationship between the normalized equilibrium beach slope, $\tan\beta/ak_o$, and the dimensionless depth, $k_o h$, for different values of the parameter $a\sigma/W$. Normal incident waves are assumed.

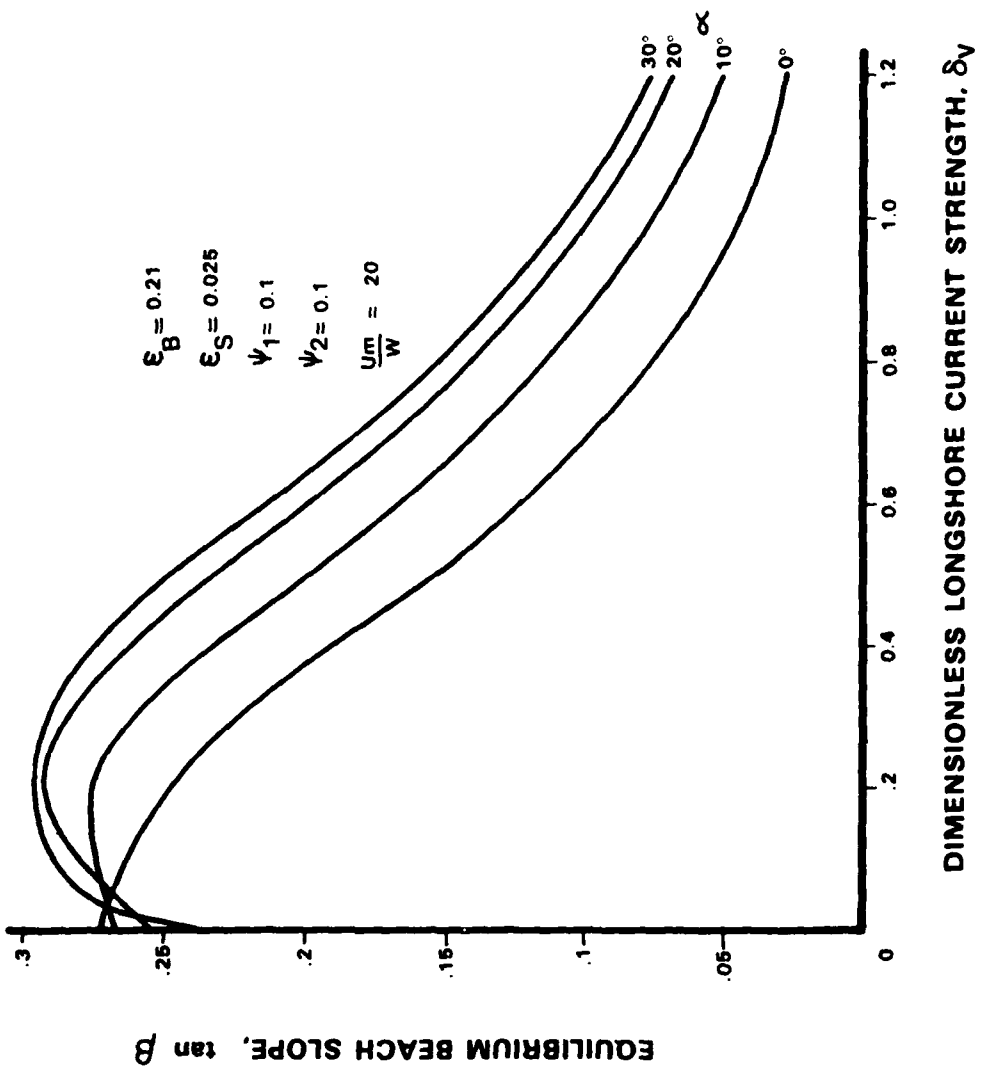

Figure 6. Relationship between the equilibrium beach slope, $\tan\beta$, and the dimensionless longshore current strength, δ_V, for different local wave angles, α.

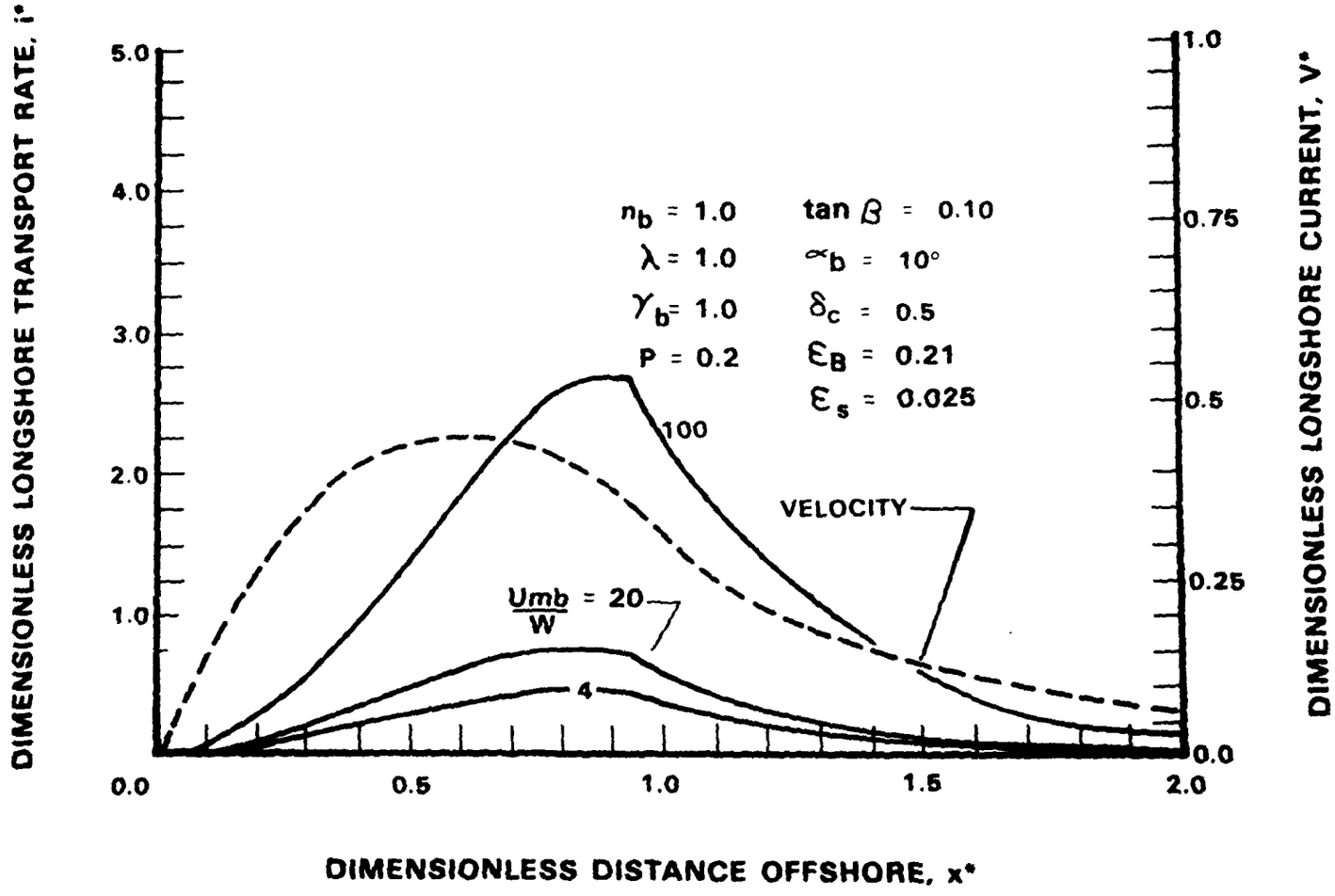

Figure 7. Dimensionless surfzone total load sediment transport and velocity profiles for different values of the velocity ratio, u_{mb}/W.

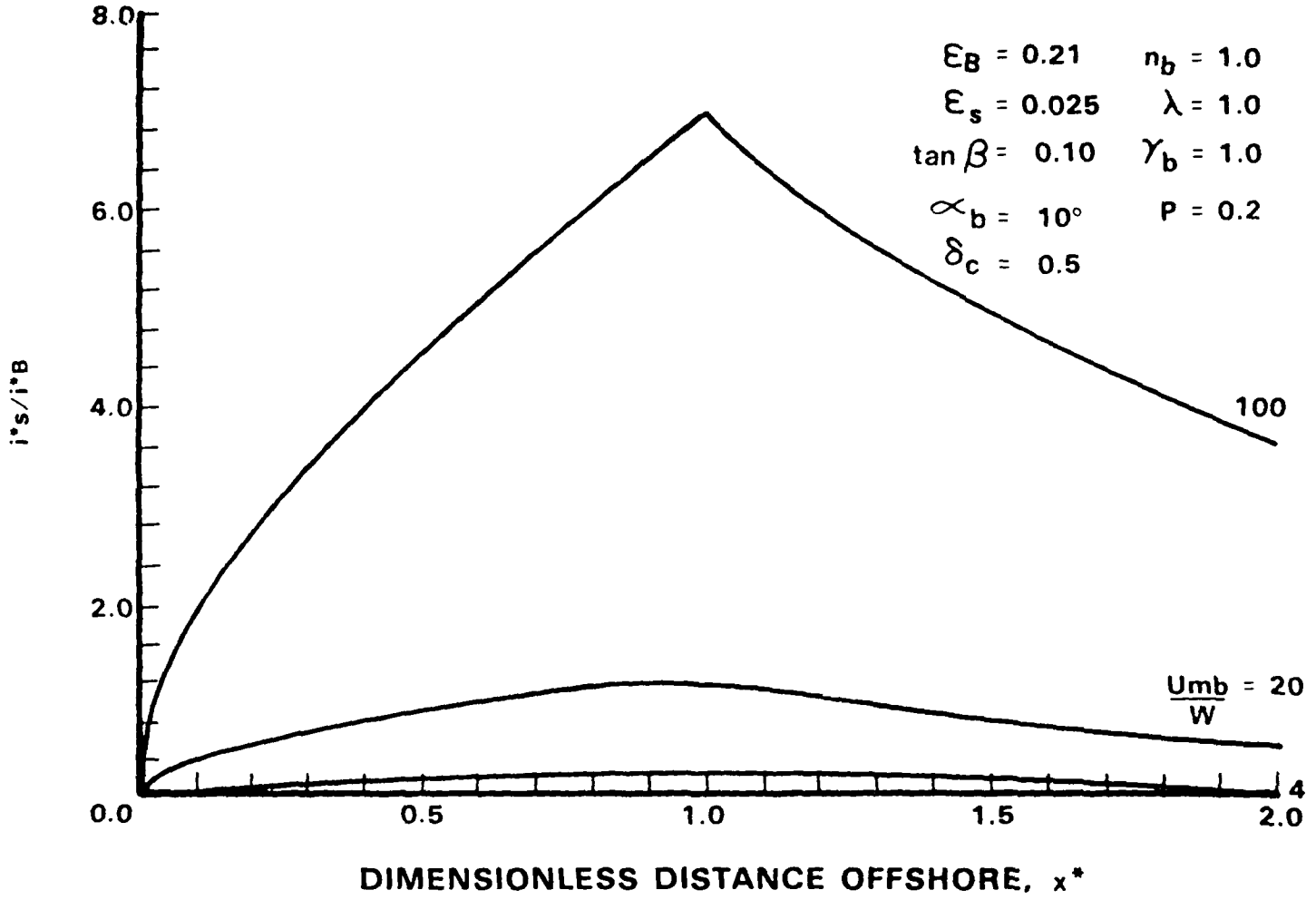

Figure 8. Surfzone distribution of the sediment transport ratio i_s^*/i_B^*, for different values of the velocity ratio u_{mb}/W.

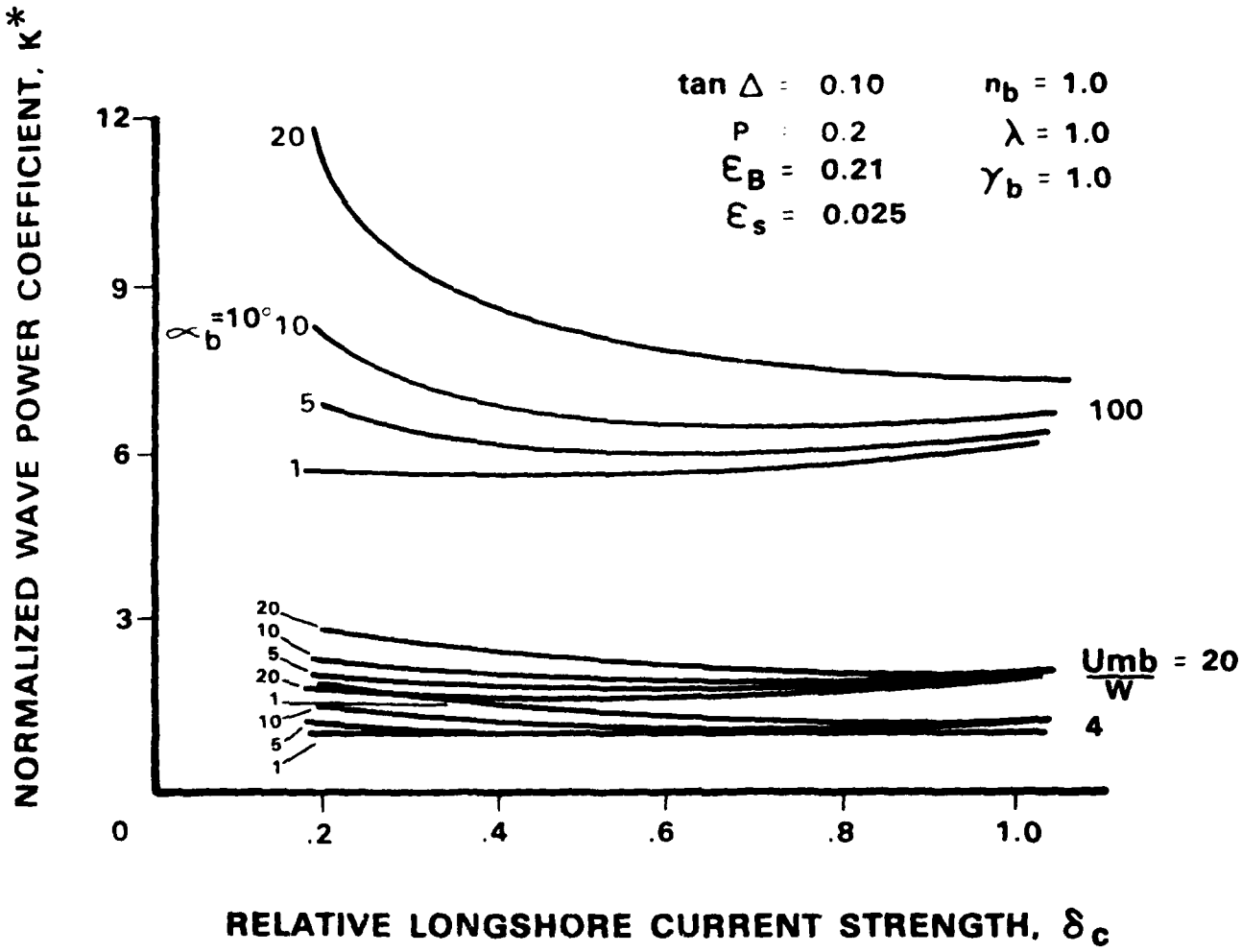

Figure 9. Relationship between the normalized wave power coefficient, K*, and the relative lonshore current strength, δ_c, for different values of the velocity ratio, u_{mb}/W.

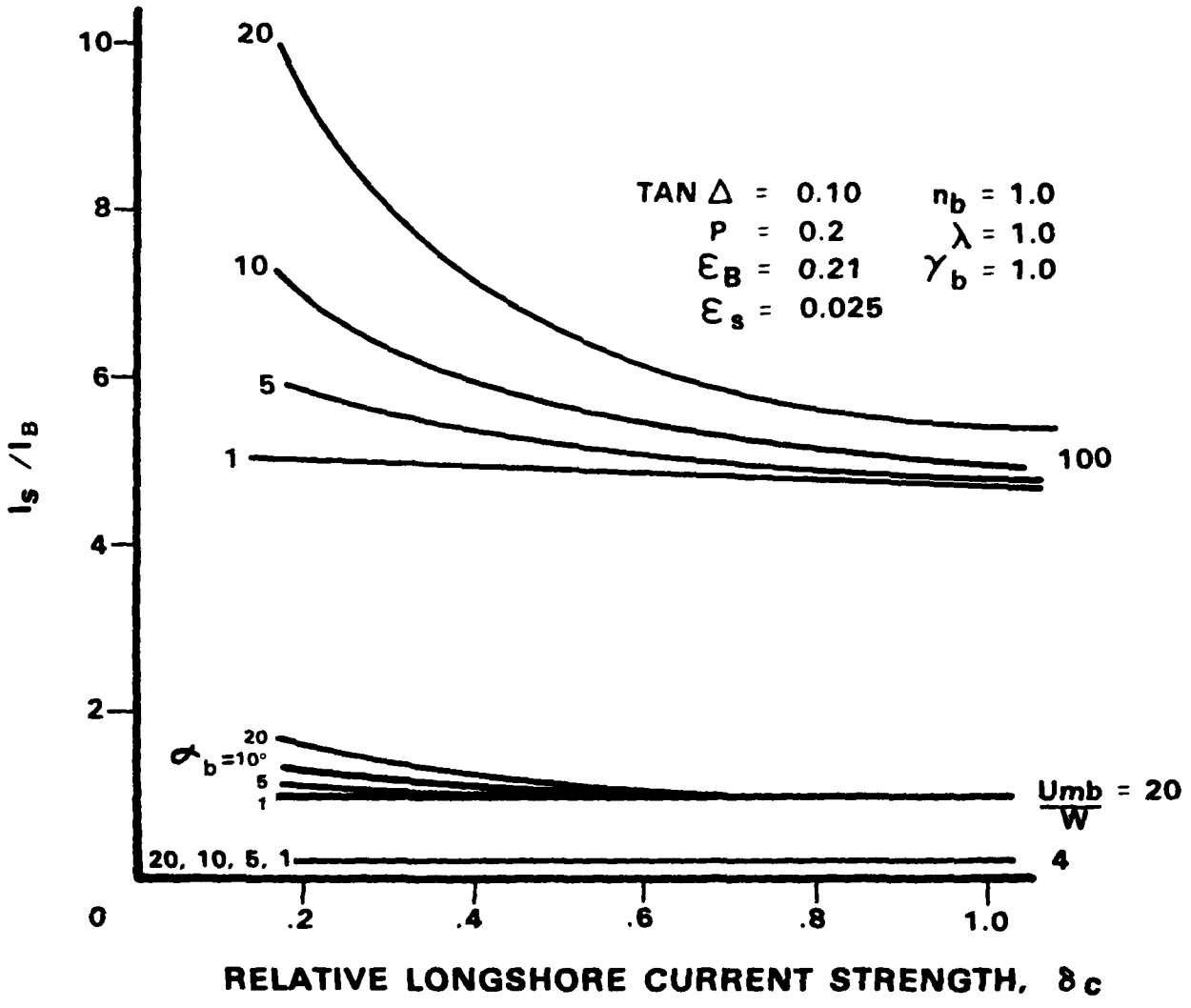

Figure 10. *Relationship* between the ratio of the sediment transport ratio, I_s/I_B, and the relative longshore current strength, δ_c, for different values of the velocity ratio u_{mb}/W.

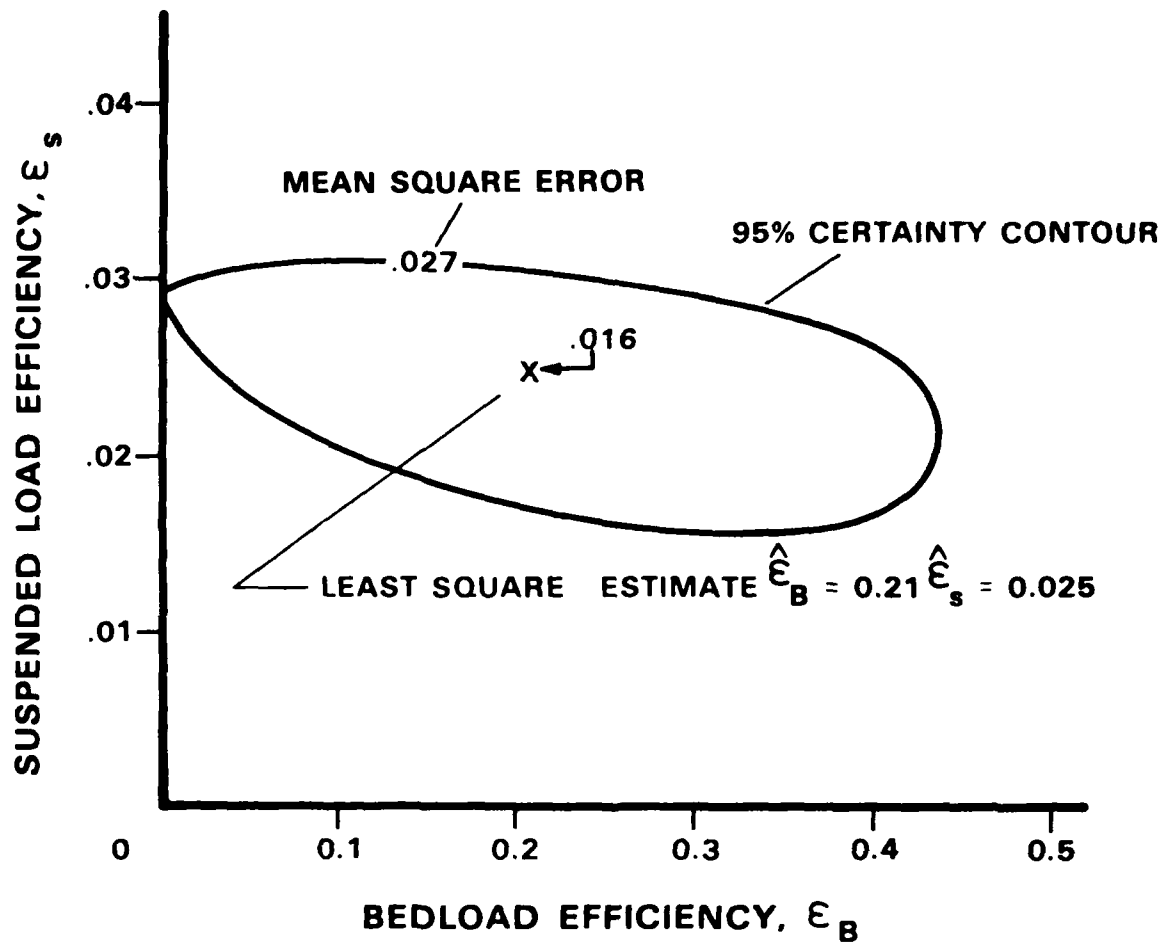

Figure 11. Least square estimates of the bedload sediment transport efficiency, $\hat{\epsilon}_B$, and the suspended sediment transport efficiency, $\hat{\epsilon}_s$, based on laboratory and field data.

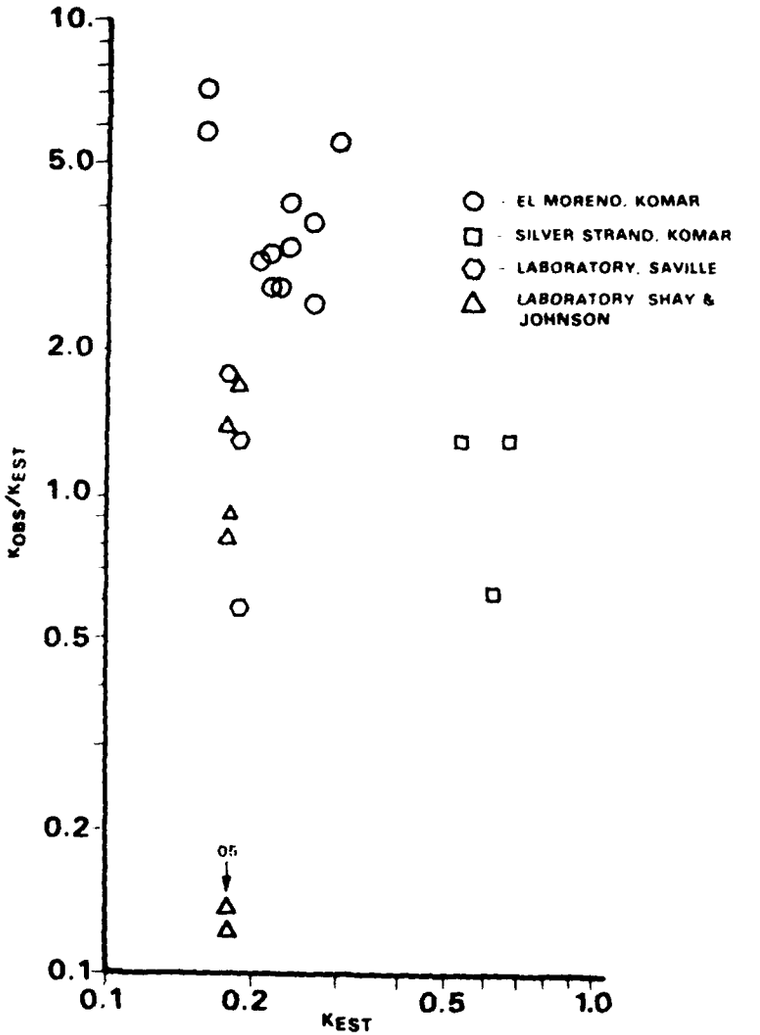

Figure 12. Comparison between the estimated and observed wave power coefficients for several laboratory and field studies.

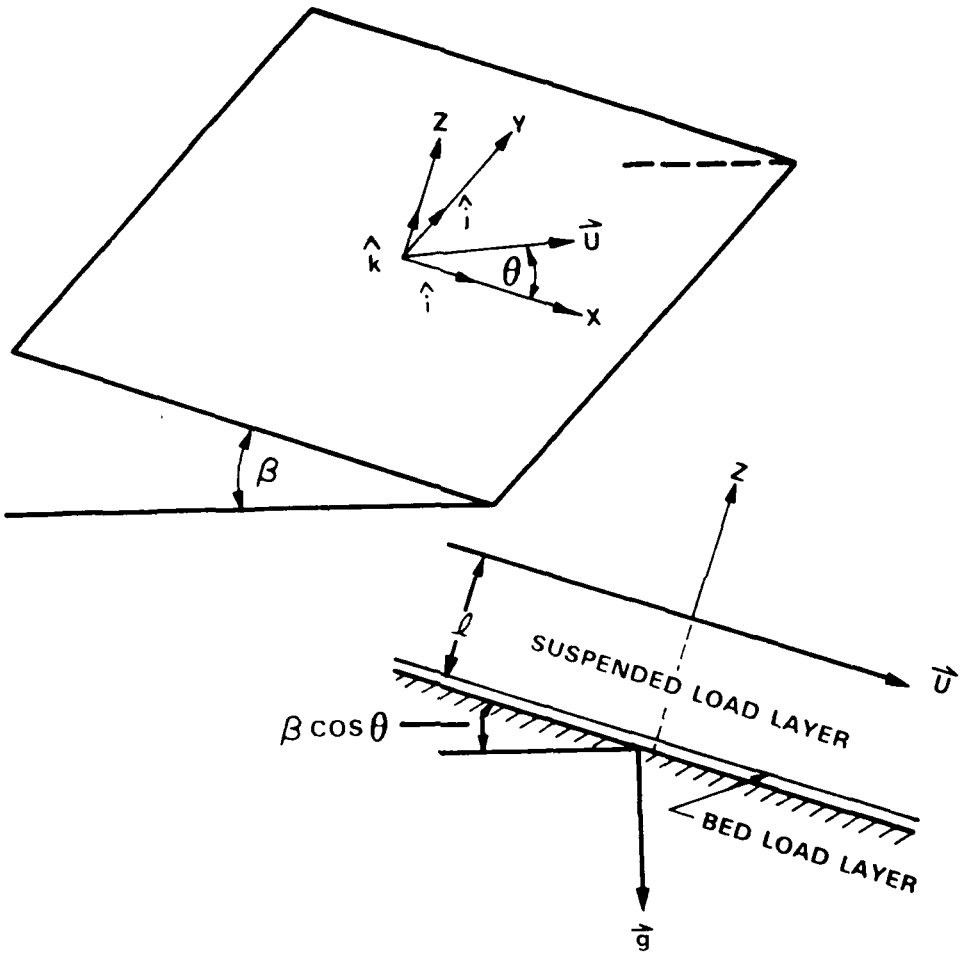

Figure 13. Schematic diagram used in developing a general form suspended sediment transport model.

Appendix

A GENERAL DERIVATION OF BAGNOLD'S SUSPENDED SEDIMENT TRANSPORT EQUATION

For simplicity, we first consider steady two-dimensional stream flow over a planar bed with slope tanβ. The water flows with velocity $\vec{u}(z)$ over a depth h. The x-coordinate is directed downslope and the z-coordinate is directed perpendicular and upward from the bed. The origin is at the base of the bed.

From geometry, the rate of energy production of the stream, ω_{stream}, is equal to

$$\omega_{stream} = \int_0^h \rho_a \, g \, \sin\beta \, \vec{u} \cdot \hat{i} \, dz \qquad (A1)$$

where ρ_a is the apparent density of the sediment-ladened water. This may be expressed as

$$\rho_a = (\rho_s - \rho)N + \rho \qquad (A2)$$

where ρ_s = density of the sediment grains
N = local volume concentration of solids
ρ = density of sediment-free water

Assuming that the suspended sediment moves downstream with approximately the local water velocity, $\vec{u}$, then Equations A1 and A2 may be combined to yield

$$\omega_{stream} = (\rho_s - \rho)\, g \sin\beta \int_0^h N\, \vec{u}\cdot\hat{i}\, dz + \omega \qquad (A3)$$

where ω is the sediment-free stream power.

Following Bagnold, we define an immersed weight suspended sediment transport rate per unit area bed, $\vec{i}_S$, as

$$\vec{i}_S = (\rho_s - \rho)\, g \cos\beta \int_0^h N\, \vec{u}\, dz \qquad (A4)$$

Bagnold (1963, 1966) assumed that the rate of energy dissipation per unit area of bed associated with this transport of sediment, ω_{sed}, is equal to the sediment load times its fall velocity, i.e.,

$$\omega_{sed} = (\rho_s - \rho)\, g \cos\beta\, W \int_0^h N\, dz \qquad (A5)$$

where W is the sediment fall velocity. Combining Equations A4 and A5, we find

$$\omega_{sed} = \frac{\left|\vec{i}_S\right| W}{\bar{u}} \qquad (A6)$$

where

$$\bar{u} = \frac{\left| \int_0^h N\, \vec{u}\, dz \right|}{\int_0^h N\, dz} \qquad (A7)$$

Bagnold's critical hypothesis is that the rate of energy dissipation associated with the suspended sediment transport, ω_{sed}, is related to the total rate of energy production of the stream, ω_{stream}, through a constant suspended load efficiency factor, ε_S, so that

$$\omega_{sed} = \varepsilon_S \omega_{stream} \tag{A8}$$

Combining Equations A3, A4, A6, and A8, we obtain an equation for the magnitude of the suspended sediment transport rate

$$\left| \vec{i}_S \right| = \varepsilon_S \frac{\bar{u}}{W} (\tan\beta \, \vec{i}_s \cdot \hat{i} + \omega) \tag{A9}$$

It should be noted that Equation A9 does not reduce to Bagnold's stream-based transport model except for negligible slopes. To see this, we rearrange Equation A9 to become

$$\left| \vec{i}_S \right| = \frac{\varepsilon_S \omega}{\left(\frac{W}{\bar{u}} - \varepsilon_S \tan\beta \right)} \tag{A10}$$

By inspection, Equation A10 differs from Bagnold's stream transport Equation 1 by the inclusion of the factor ε_S in the denominator. Conceptually this difference arises because Bagnold assumed that the stream power contribution from the suspended sediment load contributes directly to the suspended sediment transport rate instead of through an efficiency factor as in Equation A9. If Bagnold's hypothesis is correct, then Equation A9 should read

$$\left| \vec{i}_S \right| = \frac{\bar{u}}{W} (\tan\beta \, \vec{i}_s \cdot \hat{i} + \varepsilon_S \omega) \tag{A11}$$

This subtle difference between Equations A9 and A11 is negligible for the small bedslopes normally in stream flow conditions. It becomes extremely important, however, with respect to equilibrium beach slopes as seen in the main body of the paper. This is because Equation A11 (or Equation 1) predicts autosuspension conditions (infinite downslope transport rates) when $|\bar{u}|$ exceeds $W/\tan\beta$. Interestingly, this condition can be exceeded momentarily on natural sand beaches. For autosuspension to occur in the present model, however, $|\bar{u}|$ must exceed $W/(\varepsilon_s \tan\beta)$. Since $1/\varepsilon_s \cong 40$, this condition is much less apt to be met.

Although Equation A9 was developed for two-dimensional stream flow, it seems plausible that it can be modified to include the more general situation of a steady flow over a planar sloping bed having an arbitrary orientation relative to the direction of fluid flow. Under these more general conditions, the direction of the sediment transport rate need not be colinear with the direction of fluid flow. In addition to moving with the nearbottom water velocity, the downslope component of suspended sediment load can be expected to produce a downslope-directed sediment transport.

In the general case of suspended sediment transport, sediment can be expected to be distributed throughout the turbulent boundary layer region. In the case of fully developed stream flow, this is roughly the total water depth, but for oscillatory flow the boundary layer thickness is much less. Smith (1977) and Grant and Madsen (1979) show that the turbulent boundary layer thickness under waves is approximately $(u^*)_m/\sigma$, where $(u^*)_m$ is the magnitude of the oscillatory shear velocity and σ is the angular frequency of the waves. For typical nearshore wave conditions, the boundary layer thickness is on the order of several centimeters.

Within the boundary layer region, the sediment concentration increases exponentially towards the bed. Consequently, most of the sediment is found relatively near the bed. For reasons that will become evident, it is mathematically convenient to assume that most of the sediment is transported near the bed, within the logarithmic or "law of the wall" portion of the boundary layer, where the shear stress is constant. For

steady two-dimensional stream flow, the logarithmic boundary layer can be assumed to be the lower one-tenth of the stream depth (Smith and McLean, 1977). For oscillatory turbulent boundary layers, Smith (1977) concludes that the logarithmic layer thickness is 0.02 times the wave boundary layer, while Grant and Madsen (1979) assume that it is the full boundary layer thickness as defined by $(u^*)_m/\sigma$. The latter will be assumed in the present development.

Consider a steady current, $\vec{u}$, flowing over a planar bed with slope $\tan\beta$ (Figure 13). The current flows parallel to the bed and at an angle θ relative to the downslope-directed x-axis. The y-axis is directed across slope and the z-axis is directed perpendicular and upward from the bed. The origin is assumed to be at the top of the bedload layer, which is nominally a few grain diameters above the stationary bed. As discussed, the suspended sediment transport is assumed to occur relatively near the bed, as compared with the total water depth. Although in practice the local transport rate will be colinear with the local shear stress, it is assumed for simplicity that the direction of the suspended sediment transport rate is co-linear with the shear stress at the base of the suspended sediment layer.

Considering now the limited nearbottom region of suspended sediment transport and assuming that steady, nonaccelerating conditions exist, the momentum equation is

$$(\rho_s - \rho)N\vec{g} + \vec{\nabla}\cdot\vec{\vec{T}} = 0 \qquad \text{(A12)}$$

where $\vec{\vec{T}}$ is the sediment-ladened fluid stress tensor, which has been corrected for the sediment-free fluid pressure, ρgz. Boundary conditions for the flow are as follows. At the top of the suspension layer, the normal stress, T_{zz}, is zero. At the base of the suspension layer, the current exerts a shear stress, T_o, in the θ direction. Assuming, however, that the suspension layer is sufficiently small, the current-related shear stress can be assumed to be applied to the top of the suspension layer. This is equivalent to assuming that the current-related shear

stress is constant throughout the suspension layer, as is consistent with a logarithmic velocity profile. Assuming that the logarithmic boundary layer thickness is ℓ, the boundary conditions may be expressed as

$$z = \ell: \quad \begin{aligned} T_{xz} &= T_o \cos\theta \\ T_{yz} &= T_o \sin\theta \\ T_{zz} &= 0 \end{aligned} \tag{A13}$$

Integrating the x, y, and z components of Equation A12 and evaluating the integration constants with Equation A13, we obtain

$$T_{xz} = (\rho_s - \rho)\, g \sin\beta \int_z^{\ell} N\, dz + T_o \cos\theta \tag{A14}$$

$$T_{yz} = T_o \sin\theta \tag{A15}$$

$$T_{zz} = (\rho_s - \rho)\, g \cos\beta \int_z^{\ell} N\, dz \tag{A16}$$

Recognizing that the shear stress, $\vec{T}$, on the x-y plane is calculated as

$$\vec{T} = T_{xz}\, \hat{i} + T_{yz}\, \hat{j} \tag{A17}$$

the shear stress at the base of the suspension layer becomes

$$\vec{T}\Big|_{z=0} = (T_g + T_o \cos\theta)\hat{i} + T_o \sin\theta\, \hat{j} \tag{A18}$$

where T_g is the downslope component of stress due to the immersed weight of the suspended sediment and is equal to

$$T_g = (\rho_s - \rho)\, g \sin\beta \int_o^{\ell} N\, dz \tag{A19}$$

Assuming that $T_g << T_o$, which is consistent with the assumption of a small bedslope, then

$$\left|\vec{\tau}\right|_{z=0} \cong T_o + T_g \cos\theta \tag{A20}$$

Thus

$$\left.\frac{\vec{\tau}}{\left|\vec{\tau}\right|}\right|_{z=0} \cong (\cos\theta + \frac{T_g}{T_o}\sin^2\theta)\hat{i} + (\sin\theta - \frac{T_g}{T_o}\sin\theta\cos\theta)\,\hat{j} \tag{A21}$$

Noting, however, that

$$\frac{\vec{u}}{\left|\vec{u}\right|} = \cos\theta\,\hat{i} + \sin\theta\,\hat{j}$$

then

$$\left.\frac{\vec{\tau}}{\left|\vec{\tau}\right|}\right|_{z=0} = \frac{\vec{u}}{\left|\vec{u}\right|} + \frac{T_g}{T_o}(\sin^2\theta\,\hat{i} - \sin\theta\cos\theta\,\hat{j}) \tag{A22}$$

As previously mentioned, the suspended sediment transport rate is assumed to be directed parallel to $\vec{\tau}_{z=0}$, thus

$$\vec{i}_S = \left|\vec{i}_S\right| \left.\frac{\vec{\tau}}{\left|\vec{\tau}\right|}\right|_{z=0} \tag{A23}$$

Combining Equations A9, A22, and A23, we obtain to $o(\varepsilon_s^2)$

$$\vec{i}_S = \frac{\varepsilon_S}{W} \omega \vec{u} + \frac{\varepsilon_S^2}{W^2} \tan\beta \, \omega \left|\vec{u}\right| \cos\theta \, \vec{u}$$

$$+ \frac{\varepsilon_S}{W^2} \tan\beta \frac{\omega^2}{T_o} \left|\vec{u}\right| (\sin^2\theta \, \hat{i} - \sin\theta \cos\theta \, \hat{j}) \qquad \text{(A24)}$$

where it has been assumed that $\bar{u} \cong \left|\vec{u}\right|$.

Assuming next that

$$T_o = \rho c_f \left|\vec{u}\right|^2 \qquad \text{(A25)}$$

and

$$\omega = \rho \, c_f \left|\vec{u}\right|^3 \qquad \text{(A26)}$$

where c_f is the drag coefficient for the bed, then Equation A24 becomes

$$\vec{i}_S = \rho \, c_f \frac{\varepsilon_S}{W} \left|\vec{u}\right|^3 \vec{u} + \rho \, c_f \tan\beta \frac{\varepsilon_S^2}{W^2} \left|\vec{u}\right|^5 \hat{i} \qquad \text{(A27)}$$

Assuming now that the nearbottom velocity vector is a time-varying quantity, $\vec{u}_t$, and that the suspended sediment transport rate responds to the instantaneous velocity in a quasi-steady manner, a vector, $\vec{K}_{St}$, may be defined as

$$\vec{K}_{St} = \frac{\vec{i}_{St}}{\omega} \qquad \text{(A28)}$$

Thus,

$$\vec{K}_{St} = \frac{\varepsilon_S \left|\vec{u}_t\right|}{W} \left(\frac{\vec{u}_t}{\vec{u}_t} + \varepsilon_S \tan\beta \frac{\left|\vec{u}_t\right|}{W} \hat{i} \right) \tag{A29}$$

Finally, if the bed slopes in the negative $\hat{i}$-direction, Equation A29 becomes equal to Equation 9 in the main body of text.

NOMENCLATURE

a	Wave amplitude (ℓ)
C	Phase velocity (ℓ/t)
$C_1 - C_3$	Modified Longuet-Higgins constants
c_f	Bed drag coefficient
E	Wave energy (m/t^2)
g	Gravity (ℓ/t^2)
H	Wave height (ℓ)
h	Water depth (ℓ)
i	Local sediment transport rate (m/t^3)
$\vec{i}$	Local sediment transport rate vector (m/t^3)
$\hat{i}$	Unit vector in onshore direction
I_B	Spatially integrated longshore bedload sediment transport rate ($m\text{-}\ell/t^3$)
i_B	Local bedload sediment transport rate (m/t^3)
$\vec{i}_B$	Local bedload sediment transport rate vector (m/t^3)
i_c	Characteristic local longshore sediment transport rate (m/t^3)
I_ℓ	Spatially integrated, total load, longshore sediment transport rate ($m\text{-}\ell/t^3$)
I_S	Spatially integrated longshore suspended load sediment transport rate ($m\text{-}\ell/t^3$)
i_S	Local suspended sediment transport rate (m/t^3)
$\vec{i}_S$	Local suspended sediment transport rate vector (m/t^3)
$\langle i_x \rangle$	Time-averaged local on-offshore sediment transport rate (m/t^3)
$\langle i_y \rangle$	Time-averaged local longshore sediment transport rate (m/t^3)

$\langle i_y^* \rangle$	Normalized time-averaged local longshore sediment transport rate
i_θ	Local sediment transport rate in θ direction (m/t^3)
$\hat{j}$	Unit vector in longshore direction
K	Wave power coefficient
K'	Bagnold's oscillatory transport rate coefficient
K*	Normalized wave power coefficient
$K_1 - K_3$	Wave power coefficient integrals
$\vec{K}_{Bt}$	Vector bedload wave power coefficient
K_{est}	Estimated wave power coefficient
K_o	Wave power coefficient for negligible lateral mixing, longshore current strength, breaker angle, wave height, and orbital-velocity-to-fall-velocity ratio
K_{obs}	Observed wave power coefficient
$\vec{K}_{St}$	Vector suspended load wave power coefficient
k	Wave number ($1/\ell$)
k_o	Deep water wave number ($1/\ell$)
ℓ	Sediment layer thickness (ℓ)
N	Volume concentration of solids
n	Wave energy transport function
n_b	Finite breaker height factor
P	Lateral mixing parameter
P_ℓ	Longshore component of wave energy flux ($m\text{-}\ell/t^3$)
$S(\varepsilon_B, \varepsilon_S)$	Mean square error of wave power coefficient estimates
T	Wave period (t)
$\vec{\vec{T}}$, T_{ij}	Sediment-ladened fluid stress tensor (m/t^2)
T_g	Downslope component of immersed sediment weight ($m/\ell\text{-}t^2$)

T_o	Shear stress at the base of the suspension layer ($m/\ell\text{-}t^2$)
T_{zz}	Normal stress at top of the suspension layer ($m/\ell\text{-}t^2$)
t	Time (t)
$\bar{u}$	Mean velocity magnitude (ℓ/t)
$\tilde{u}$	Oscillatory surfzone velocity (ℓ/t)
$\vec{u}$	Total vector velocity (ℓ/t)
(u3)*	Velocity magnitude integral
(u5)*	Velocity magnitude integral
u_m	Oscillatory velocity magnitude (ℓ/t)
$(u^*)_m$	Oscillatory shear velocity magnitude (ℓ/t)
u_θ	Mean water velocity in θ direction (ℓ/t)
v	Longshore current magnitude (ℓ/t)
v*	Dimensionless longshore current distribution
v_c	Characteristic longshore current magnitude (ℓ/t)
W	Sediment full velocity (ℓ/t)
x	Shore normal coordinate (ℓ)
x*	Dimensionless surfzone position
x_S	Shoreline position (ℓ)
x_B	Breaker position (ℓ)
y	Longshore coordinate (ℓ)
z	Vertical coordinate (ℓ)

GREEK ALPHABET

α	Wave angle (deg)
α_b	Breaker angle (deg)
$\tan\beta$	Bed slope
Γ	Lateral mixing coefficient

γ	Ratio of wave height to water depth
Δ	Bed angle modified for wave setup (deg)
δ	Dimensionless steady current strength
δ_c	Relative longshore current strength
δ_u	Dimensionless onshore current strength
δ_v	Dimensionless longshore current strength
ε_B	Bedload efficiency
ε_S	Suspended load efficiency
θ	Steady current angle (deg)
λ	Finite longshore current factor
ρ	Fluid density (m/ℓ^3)
ρ_a	Apparent density of suspension (m/ℓ^3)
ρ_s	Sediment grain density (m/ℓ^3)
σ	Wave frequency (1/t)
$\vec{\tau}$	Bed shear stress vector ($m/\ell\text{-}t^2$)
ϕ	Internal angle of friction (deg)
ψ_1	Velocity skewness factor
ψ_2	Velocity skewness factor
ω	Local rate of energy dissipation production (m/t^3)
ω_{sed}	Rate of energy dissipation associated with the suspended sediment transport (m/t^3)
ω_{stream}	Rate of energy production of a stream (m/t^3)

OTHER SYMBOLS

$< >$	Time average quantity
$\lvert\ \rvert$	Absolute value
$\rightarrow$	Vector quantity

SUBSCRIPTS

b	Break point quantity
t	Time varying quantity

DISTRIBUTION LIST

AFB AUL LSE 63-465, Maxwell AL; CESCH, Wright-Patterson; Stinfo Library, Offutt NE
ARCTICSUBLAB Code 54, San Diego, CA
ARMY BMDSC-RE (H. McClellan) Huntsville AL; DAEN-MPE-D Washington DC
ARMY COASTAL ENGR RSCH CEN Fort Belvoir VA; R. Iachowski, Fort Belvoir VA
ARMY COE Philadelphia Dist (LIBRARY) Philadelphia, PA
ARMY CORPS OF ENGINEERS MRD-Eng. Div., Omaha NE; Seattle Dist Library, Seattle WA
ARMY CRREL A. Kovacs, Hanover NH
ARMY DARCOM Code DRCMM-CS Alexandria VA
ARMY ENG WATERWAYS EXP STA Library, Vicksburg MS
ARMY ENGR DIST, Library, Portland OR
ARMY ENVIRON. HYGIENE AGCY HSE-EW Water Qual Eng Div Aberdeen Prov Grnd MD
ARMY MAT SYS ANALYSIS ACT Code DRXSY-CM (M Ogorzalek) Aberdeen Proving Grnd MD
ARMY MATERIALS & MECHANICS RESEARCH CENTER Dr. Lenoe, Watertown MA
ARMY MOBIL EQUIP R&D COM DRDME-MR (J. Sargent) Ft. Belvoir VA
ARMY MTMC Trans Engr Agency MTT-CE, Newport News, VA
ARMY TRANSPORTATION SCHOOL Code ATSPO CD-TE Fort Eustis, VA
ARMY TRNG & DOCTRINE CMD Code ATCD-SL Fort Monroe, VA
ASST SECRETARY OF THE NAVY Spec. Assist Submarines, Washington DC
BUREAU OF RECLAMATION Code 1512 (C. Selander) Denver CO
CINCLANT Civil Engr. Supp. Plans. Ofr Norfolk, VA
CINCPAC Fac Engrng Div (J44) Makalapa, HI
CNM Code 03462, Washington DC; Code 043 Washington DC; Code MAT-04, Washington, DC; MAT-0718, Washington, DC; NMAT - 044, Washington DC
CNO Code NOP-964, Washington DC; Code OP 323, Washington DC; Code OP 405, Washington DC; Code OP 405, Washington, DC; Code OP 414, Washington DC; Code OP 97 Washington DC; Code OP 97 Washington, DC; Code OP 987 Washington DC; Code OP323 Washington DC; Code OPNAV 09B24 (H); Code OPNAV 22, Wash DC; Code OPNAV 23, Wash DC; OP-411F, Wash DC; OP987J (J. Boosman), Pentagon
COMCBPAC Operations Off, Makalapa HI
COMNAVBEACHPHIBREFTRAGRU ONE San Diego CA
COMNAVMARIANAS Code N4, Guam
COMOCEANSYSPAC SCE, Pearl Harbor HI
COMSUBDEVGRUONE Operations Offr, San Diego, CA
NAVSURFLANT Norfolk, VA
NAVSURFPAC Code N-4, Coronado
COMOPTEVFOR CMDR, Norfolk, VA; Code 705, San Diego, CA
DEFFUELSUPPCEN DFSC-OWE (Grafton) Alexandria, VA; DFSC-OWE (Term Engrng) Alexandria, VA
DLSIE Army Logistics Mgt Center, Fort Lee, VA
DNA STTL, Washington DC
DTIC Defense Technical Info Ctr/Alexandria, VA
DTNSRDC Anna Lab (Code 119) Annapolis MD; Anna Lab (Code 1568) Annapolis MD
FMFLANT CEC Offr, Norfolk VA
FMFPAC CG(FEO) Camp Smith, HI
GSA Assist Comm Des & Cnst (FAIA) D R Dibner Washington, DC
LIBRARY OF CONGRESS Washington, DC (Sciences & Tech Div)
MARINE CORPS BASE 1st For Serv Supp Grp (CSS-5) Camp Pendleton CA; PWO, Camp S. D. Butler, Kawasaki Japan
MCAS Facil. Engr. Div. Cherry Point NC; Facs Maint Dept - Operations Div, Cherry Point
MCDEC M&L Div Quantico VA; NSAP REP, Quantico VA
MCRD PWO, San Diego Ca
MILITARY SEALIFT COMMAND Washington DC
NAF PWO, Atsugi Japan
NARF Equipment Engineering Division (Code 61000), Pensacola, FL
NAS Dir. Util. Div., Bermuda; Lead. Chief. Petty Offr. PW/Self Help Div, Beeville TX; PW (J. Maguire), Corpus Christi TX; PWD - Engr Div, Oak Harbor, WA; PWD Maint. Div., New Orleans, Belle Chasse LA; PWD, Code 1821H (Pfankuch) Miramar, SD CA; PWO Belle Chasse, LA; PWO Key West FL; PWO, Glenview IL; ROICC Key West FL, SCE Norfolk, VA; Shore Facil. Ofr Norfolk, VA
NATL BUREAU OF STANDARDS Kovacs, Washington, D.C.
NATL RESEARCH COUNCIL Naval Studies Board, Washington DC

NAVACT PWO, London UK
NAVAEROSPREGMEDCEN SCE, Pensacola FL
NAVAIRDEVCEN Code 813, Warminster PA
NAVCHAPGRU CO Williamsburg VA
NAVCOASTSYSCEN Code 772 (C B Koesy) Panama City FL
NAVCOASTSYSTCTR CO, Panama City FL; Code 715 (J Quirk) Panama City, FL; Code 715 (J. Mittleman) Panama City, FL; Library Panama City, FL
NAVCOMMAREAMSTRSTA SCE, Wahiawa HI; SCE Unit 1 Naples Italy
NAVCOMMSTA Code 401 Nea Makri, Greece; PWD-ENG Div Dir Washington, DC; PWO, Exmouth, Australia
NAVCONSTRACEN Curriculum Instr. Stds Offr, Gulfport MS
NAVEDTRAPRODEVCEN Technical Library, Pensacola, FL
NAVELEXSYSCOM Code PME 124-61, Washington, DC; PME 124-612, Wash DC
NAVEODFAC Code 605, Indian Head MD
NAVFAC PWO, Centerville Bch, Ferndale CA
NAVFACENGCOM Code 03T (Essoglou) Alexandria, VA; Code 043 Alexandria, VA; Code 044 Alexandria, VA; Code 0451 (P W Brewer) Alexandria, Va; Code 0453 (D Potter) Alexandria, VA; Code 0453C, Alexandria, VA; Code 04A1 Alexandria, VA; Code 06, Alexandria VA Code 0632, Alexandria, VA; Code 1113 (M. Carr) Alexandria, VA; Code 1113 (T. Stevens) Alexandria, VA; Morrison Yap Caroline Is
NAVFACENGCOM - CHES DIV, Code 405 Wash, DC; Code 407 (D Scheesele) Washington DC; Code FPO-1C Washington DC; FPO-1 Washington, DC; FPO-1EA5 Washington DC
NAVFACENGCOM - LANT DIV, Eur. BR Deputy Dir, Naples Italy; RDT&ELO 102, Norfolk VA
NAVFACENGCOM - NORTH DIV, (Boretsky) Philadelphia, PA; CO, Code 09P Philadelphia PA; Code 1028, RDT&ELO, Philadelphia PA; ROICC, Contracts, Crane IN
NAVFACENGCOM - PAC DIV, CODE 09P PEARL HARBOR HI; Code 2011 Pearl Harbor, HI; Code 402, RDT&E, Pearl Harbor HI; Commander, Pearl Harbor, HI
NAVFACENGCOM - SOUTH DIV, Code 90, RDT&ELO, Charleston SC
NAVFACENGCOM - WEST DIV, Code 04B San Bruno, CA; O9P/20 San Bruno, CA, RDT&ELO Code 2011 San Bruno, CA
NAVFACENGCOM CONTRACT Eng Div dir, Southwest Pac, Manila, PI; OICC, Southwest Pac, Manila, PI; OICC/ROICC, Balboa Panama Canal; ROICC, Keflavik, Iceland; ROICC, NAS, Corpus Christi, TX
NAVFORCARIB Commander (N42), Puerto Rico
NAVMAG SCE, Subic Bay, R.P.
NAVOCEANO Library Bay St. Louis, MS
NAVOCEANSYSCEN Code 41, San Diego, CA; Code 4473 Bayside Library, San Diego, CA; Code 4473B (Tech Lib) San Diego, CA; Code 52 (H. Talkington) San Diego CA; Code 5204 (J. Stachiw), San Diego, CA; Code 5214 (H. Wheeler), San Diego CA; Code 5221 (R.Jones) San Diego Ca; Code 5311 (Bachman) San Diego, CA; Hawaii Lab (R Yumori) Kailua, HI; Hi Lab Tech Lib Kailua HI
NAVPGSCOL C. Morers Monterey CA; Code 61WL (O. Wilson) Monterey CA; E. Thornton, Monterey CA
NAVPHIBASE CO, ACB 2 Norfolk, VA; COMNAVBEACHGRU TWO Norfolk VA; Code S3T, Norfolk VA; Dir, Amphib. Warfare Brd Staff, Norfolk, VA; Harbor Clearance Unit Two, Little Creek, VA; SCE, Coronado, San Diego CA
NAVREGMEDCEN SCE (D. Kaye); SCE, Guam
NAVSCOLCECOFF C35 Port Hueneme, CA
NAVSCSOL PWO, Athens GA
NAVSEASYSCOM Code SEA OOC Washington, DC; SEA 04E (L Kess) Washington, DC
NAVSECGRUACT PWO, Adak AK
NAVSHIPYD Bremerton, WA (Carr Inlet Acoustic Range); Code 202.5 (Library) Puget Sound, Bremerton WA; Code 380, Portsmouth, VA; Code 440 Portsmouth NH; Code 440, Puget Sound, Bremerton WA; Tech Library, Vallejo, CA
NAVSTA Dir Engr Div, PWD, Mayport FL; PWD (LTJG.P.M. Motolenich), Puerto Rico; PWO, Mayport FL, Utilities Engr Off. Rota Spain
NAVTECHTRACEN SCE, Pensacola FL
NAVWPNCEN Code 2636 (W. Bonner), China Lake CA; Code 3803 China Lake, CA
NAVWPNSTA PW Office Yorktown, VA
NAVWPNSTA PWD - Maint. Control Div., Concord, CA; PWO, Charleston, SC; PWO, Seal Beach CA
NAVWPNSUPPCEN Code 09 Crane IN
NCTC Const. Elec. School, Port Hueneme, CA
NCBC Code 10 Davisville, RI; Code 15, Port Hueneme CA; Code 155, Port Hueneme CA; Code 156, Port Hueneme, CA; Code 1571, Port Hueneme, CA
NCBU 411 OIC, Norfolk VA
NCR 20, Commander; 30th Det, OIC, Diego Garcia I

NMCB 74, CO; FIVE, Operations Dept
NOAA (Dr. T. Mc Guinness) Rockville, MD; Library Rockville, MD
NORDA Code 410 Bay St. Louis, MS; Code 440 (Ocean Rsch Off) Bay St. Louis MS
NRL Code 5800 Washington, DC; Code 5843 (F. Rosenthal) Washington, DC, Code 8441 (R.A. Skop), Washington DC
NROTC J.W. Stephenson, UC, Berkeley, CA
NSD SCE, Subic Bay, R.P.
NTC OICC, CBU-401, Great Lakes IL
NUCLEAR REGULATORY COMMISSION T.C. Johnson, Washington, DC
NUSC Code 131 New London, CT; Code 332, B-80 (J. Wilcox) New London, CT; Code EA123 (R.S. Munn), New London CT; Code TA131 (G. De la Cruz), New London CT
OFFICE SECRETARY OF DEFENSE ASD (MRA&L) Code CSS CC Washington, DC
ONR (Scientific Dir) Pasadena, CA; Central Regional Office, Boston, MA; Code 481, Bay St. Louis, MS; Code 485 (Silva) Arlington, VA; Code 700F Arlington VA
PHIBCB 1 P&E, San Diego, CA; 1, CO San Diego, CA; 1, CSWC D Wellington, San Diego, CA
PMTC EOD Mobile Unit, Point Mugu, CA; Pat. Counsel, Point Mugu CA
PWC CO Norfolk, VA; CO, (Code 10), Oakland, CA; CO, Great Lakes IL; CO, Pearl Harbor HI; Code 10, Great Lakes, IL; Code 120, Oakland CA; Code 120C, (Library) San Diego, CA; Code 128, Guam; Code 154, Great Lakes, IL; Code 30C, Norfolk, VA; Code 30C, San Diego, CA; Code 400, Great Lakes, IL; Code 400, Pearl Harbor, HI; Code 400, San Diego, CA; Code 420, Great Lakes, IL; Code 420, Oakland, CA; Code 700, Great Lakes, IL; Code 700, San Diego, CA
SUPANX PWO, Williamsburg VA
UCT ONE OIC, Norfolk, VA; OIC, Port Hueneme CA
US DEPT OF INTERIOR Bur of Land Mngmnt Code 583 (T F Sullivan) Washington, DC
US GEOLOGICAL SURVEY Off. Marine Geology, Piteleki, Reston VA
US NAVAL FORCES Korea (ENJ-P&O)
USCG (G-MP-3/USP/82) Washington Dc; (Smith), Washington, DC
USCG R&D CENTER CO Groton, CT; D. Motherway, Groton CT; Tech. Dir. Groton, CT
USDA Forest Service Reg 3 (R. Brown) Albuquerque, NM
USNA Civil Engr Dept (R. Erchyl) Annapolis MD; Ocean Sys. Eng Dept (Dr. Monney) Annapolis, MD; PWD *Engr. Div. (C. Bradford) Annapolis* MD
WATER & POWER RESOURCES SERVICE (Smoak) Denver, CO


DATE
ILME